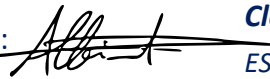




PAZ-TSX-CSK Intercomparison Quality Assessment Summary

Author(s):  **Jorge Jorge Ruiz, Juval Cohen**
Task 3 Mission Experts

Approval:  **Davide Giudici, Aresys**
Task 3 Lead

Accepted:  **Clement Albinet**
ESA Technical Officer

AMENDMENT RECORD SHEET

The Amendment Record Sheet below records the history and issue status of this document.

ISSUE	DATE	REASON
0.1	7/12/2021	Preliminary version
1.0	7/3/2022	First official version
2.0	4/4/2022	Revised after comments from ESA

ACRONYMS

AEP	Antenna Elevation Pattern
ALE	Absolute Localization Error
CR	Corner Reflector
CSK	Cosmo-SkyMed
DEM	Digital Elevation Model
DGM	Detected Ground Multilook
ENL	Equivalent Number of Looks
FMI	Finnish Meteorological Institute
HI	Himage
HR	Huge Region
HS	High Resolution Spotlight
IRF	Impulse Response Function
ISLR	Integrated Side Lobe Ratio
MGD	Multilook Ground Detected
NA	Not Applicable
NESZ	Noise Equivalent Sigma Zero
PSLR	Peak Side Lobe Ration
RD	Reference Document
SAR	Synthetic Aperture Radar
SC	ScanSAR
SCS	Single-look Complex Slant



SL	Spotlight
SM	StripMap
SSC	Single look Slant range Complex
STD	Standard Deviation
SQT	SAR Quality Toolbox
TSX	TerraSAR-X
WR	Wide Region

TABLE OF CONTENTS

AMENDMENT RECORD SHEET	2
ACRONYMS	2
1. EXECUTIVE SUMMARY	5
2. MISSION ASSESSMENT OVERVIEW	6
2.1 Product Information	6
2.2 Validation.....	8
3. DETAILED ASSESSMENT	10
3.1 IRF Analysis	12
3.1.1 PAZ.....	17
3.1.2 TSX.....	18
3.1.3 CSK.....	20
3.1.4 Intercomparison	21
3.2 Equivalent Number of Looks (ENL).....	22
3.2.1 PAZ.....	23
3.2.2 TSX.....	24
3.2.3 CSK.....	25
3.2.4 Intercomparison	26
3.3 Noise Equivalent Sigma Zero.....	26
3.3.1 PAZ.....	27
3.3.2 TSX.....	28
3.3.3 CSK.....	28
3.3.4 Intercomparison	29
3.4 Antenna Elevation Pattern	30
3.4.1 PAZ.....	30
3.4.2 TSX.....	31
3.4.3 CSK.....	33
3.4.4 Intercomparison	35
4. CONCLUSIONS	36
REFERENCES	37

1. EXECUTIVE SUMMARY

An intercomparison of the SAR quality parameters of the PAZ satellite, the TanDEM-X satellites (TerraSAR-X and TanDEM-X), and the Cosmo-SkyMed (CSK) constellation was performed within the EDAP assessment activity by the Finnish Meteorological Institute (FMI). The Cosmo SkyMed Second Generation (CSG) was already available at the time of writing this report, but only the first-generation CSK data were included. The PAZ spacecraft is based on the TerraSAR-X platform, with a total mass of ~1350 kg. The PAZ mission is a dual-use mission (civil and defence) funded and owned by the Spanish Ministry of Defence and managed by Hisdesat (Hisdesat Servicios Estratégicos, S.A.), a Spanish private communications company. TerraSAR-X and its twin satellite TanDEM-X are almost identical, having a total mass and dimensions very similar to PAZ. Both TerraSAR-X and TanDEM-X satellites are hereafter addressed in this document as TSX. The CSK constellation consists of four identical satellites, with a total mass of 1700 kg each. PAZ and TSX fly at 514 km altitude, while CSK satellites at 619.6 km altitude. Due to the very similar properties of PAZ and TSX, the quality of their data is expected to be in a similar level. Chapter 2 of this document summarizes the properties of the analysed PAZ, TSX and CSK data, and the results of the intercomparison performed in this activity using the test data delivered for the EDAP project. Chapter 3 provides more detailed explanations on the methods and the results of the data analysis and intercomparison. The quality values reported in the data provider documentation are used as an additional reference when evaluating and comparing the results measured for PAZ, TSX and CSK data.

An assessment of the essential quality parameters of SAR, such as spatial resolution, PSLR, ISLR, localization error, equivalent number of looks (ENL), noise equivalent sigma zero (NESZ) and antenna elevation pattern (AEP) was performed by FMI for the PAZ, TSX and CSK data. Representative datasets collected by these satellites from various test sites, including distributed targets and point targets were used. Data of the ScanSAR (SC), StripMap (SM), Spotlight (SL) and High Resolution Spotlight (HS) imaging modes were analysed for PAZ and TSX, while for CSK only the SC and SM modes. The product type of the analysed data was single look slant range complex (SSC or SCS) for SM, SL, and HS imaging modes, and multilooked ground range detected (MGD or DGM) for the SC imaging mode. The measured quality parameters were intercompared between PAZ, TSX and CSK, while considering the values provided in the PAZ, TSX and CSK documentation as an additional reference. The data assessment was mostly performed using the SAR Quality Toolbox (SQT) dedicated for the assessment of SAR data quality, developed by Aresys (<https://www.aresys.it/end-to-end-simulation/>). The SNAP software distributed by ESA was also used in some cases. In our previous evaluation of the PAZ data in RD-6, the quality of the PAZ test data was found to be generally in a good agreement with the values provided by Hisdesat in the product documentation. The intercomparison of the PAZ data quality with TSX and CSK presented in this document confirms and even strengthens the good results obtained in RD-6. In all evaluated aspects, PAZ data showed overall either similar or better quality than TSX and CSK.

In the IRF analysis the spatial resolution, the level of side lobes with respect to the main lobe (PSLR and ISLR), and the localization accuracy of the datasets were evaluated. The measured results showed similar quality of PAZ and TSX, with somewhat better quality of PAZ concerning localization accuracy, but somewhat better quality of TSX concerning the side lobes in range direction. The available CSK data showed generally weaker performance than PAZ and TSX concerning the PSLR, ISLR, and localization accuracy. The ENL analysis from the glaciers and the desert indicated correct radiometric processing of the PAZ, TSX and CSK data, but the ENL measured over rainforests was lower than the ideal value. Although rainforests are considered spatially homogeneous for the X-band microwaves, they may not be homogeneous enough in the spatial scale required for a proper ENL calculation. The NESZ was evaluated over low backscatter areas of smooth water and desert surfaces. The measured NESZ of PAZ was usually somewhat lower than of TSX. CSK showed better performance with lower measured NESZ values than for PAZ and TSX, especially for the SC mode. The AEP correction applied by the data provider during the SAR data processing was evaluated by analysing data from the Amazonas Rainforest. Based on the results obtained in this work, the AEP correction was generally more successful for PAZ compared to TSX and CSK.

2. MISSION ASSESSMENT OVERVIEW

2.1 Product Information

Table 1: Basic details of the data products included in the assessment.

Product Details			
	PAZ	TerraSAR-X / TanDEM-X	Cosmo-SkyMed
Product Name	Product file names contain information on the processing mode (e.g. SSC, MGD), imaging mode, polarization, antenna receive configuration (single or dual), and timing of acquisitions (start and stop). Example: PAZ1_SAR_SSC_SL_D_SRA_20180924T034217_20180924T034219	Product file names contain information on the processing mode (e.g. SSC, MGD), imaging mode, polarization, antenna receive configuration (single or dual), and timing of acquisitions (start and stop). Example: TDX1_SAR_SSC_SM_S_SRA_20210218T165349_20210218T165354	Product file names contain information on the satellite number, processing mode (e.g. SCS, DGM), imaging mode, polarization, antenna receive configuration (single or dual), and timing of acquisitions (start and stop). Example: CSKS2_SCS_B_HI_04_HH_RD_SF_20150427192048_20150427192056
Sensor Name	PAZ	TSX / TDX	CSK
Sensor Type	X-band SAR	X-band SAR	X-band SAR
Mission Type	Single satellite	Dual satellite constellation	Constellation of four satellites
Mission Orbit	Sun Synchronous	Sun Synchronous	Sun Synchronous
Product Version Number	v1.2, v1.6	v4.11	v01.04.24, v4.0.12
Processing level of product	Level 1b	Level 1b	Level 1b
Measured Quantity Name	Radar backscatter	Radar backscatter	Radar backscatter
Measured Quantity Units	dB	dB	dB
Stated Measurement Quality – Absolute radiometric accuracy	0.3 - 0.63 dB depending on acquisition mode	0.6 dB	1 dB
Spatial Resolution (range X azimuth) [m]	ScanSAR MGD: 16.8-18.2 X 17.7-18.2 Stripmap single polarization: 1.1 X 3.01, 150 MHz bandwidth Spotlight single polarization: 1.18 X 1.46, 150 MHz bandwidth HR Spotlight single polarization: 0.6 X 1.05, 300 MHz bandwidth	ScanSAR MGD: 17.0-19.2 X 18.5-19.2 Stripmap single polarization: 1.2 X 3.3, 150 MHz bandwidth Spotlight single polarization: 1.2 X 1.7, 150 MHz bandwidth HR Spotlight single polarization: 0.6 X 1.1, 300 MHz bandwidth	ScanSAR HR, DGM: 100 X 100 ScanSAR WR, DGM: 30 X 30 Stripmap HI, SCS: 2.6-3.0 X 2.4-2.6

<p>Spatial Coverage (range X azimuth) [km]</p>	<p>ScanSAR: 100 X 150 Stripmap single polarization: 30 X 50 Spotlight single polarization: 10 X 10 HR Spotlight single polarization: 6-10 X 5 (range size depends on incidence angle)</p>	<p>ScanSAR: 100 X 150 Stripmap single polarization: 30 X 50 Spotlight single polarization: 10 X 10 HR Spotlight single polarization: 5-10 X 5 (range size depends on incidence angle)</p>	<p>ScanSAR HR, DGM: 170- 240 X 200 ScanSAR WR, DGM: 100- 160 X 100 Stripmap HI, SCS: 40 X 40</p>
<p>Temporal Resolution</p>	<p>Repeat period of 11 days. Revisit time of up to 70 hours near the equators and up to 35 hours outside latitudes -35 ... 35. Maximum of 100 images per day.</p>	<p>Repeat period of 11 days for a single satellite.</p>	<p>Repeat period of 16 days for a single satellite. Revisit time of 11 hours for the 4-satellite full constellation.</p>
<p>Temporal Coverage</p>	<p>Launched in February 2018, expected lifetime 7 years</p>	<p>Launch of TSX in June 2007 and TDX in June 2010. Both with 5.5 years nominal lifetime.</p>	<p>CSK1-CSK4 launched between June 2007 and Nov 2010. Planned satellite lifetime 5 years.</p>
<p>Point of Contact</p>	<p>Address: Hisdesat Servicios Estratégicos, SA Paseo de la Castellana 149, 5th floor. Telephone: +34 914490149 Email: PAZ@hisdesat.es</p>	<p>Telephone: +49 7545 8 4344 Email: terrasar- x@airbus.com</p>	<p>Address: Via Tiburtina, 965, 00156 Rome, Italy Telephone: +39 06 40791 Email: info@e-geos.it</p>

2.2 Validation

Validation Activity #1	
Independently Assessed?	Yes
<i>Reference Data Representativeness</i>	
Summary	<i>Reference measurements assessed are well representative of the satellite measurements, covering a reasonable range of PAZ, TSX and CSK satellite's measurements. The total number of assessed SAR scenes is 117, including images from corner reflector sites for IRF and localization error analyses, as well as low backscatter images from water and desert areas, and images from homogenous targets in Amazonas rainforest and Antarctica glacier for radiometric analyses. Analysed PAZ and TSX products included data of the HS, SL, SM and SC imaging modes, and analysed CSK products included data of the SM and SC imaging modes. The reference datasets enable a proper assessment and an intercomparison between PAZ and TSX for all imaging modes, and between PAZ and CSK for the SM and SC modes. The most essential quality parameters in SAR are assessed, such as spatial resolution, geolocation accuracy, PSLR, ISLR, ENL, NESZ and AEP.</i>
Reference	<i>Chapter 3</i>
<i>Validation Method</i>	
Summary	<i>The methodology enables an assessment of the relevant SAR quality parameters for the test datasets, and an intercomparison between the measured quality parameters of the PAZ, TSX and CSK data products. The quality values provided in the PAZ, TSX and CSK documentation were used as an additional reference when assessing the quality of the products. The validation was performed mainly with a dedicated SAR quality analysis toolbox developed by Aresys, and in some cases the SNAP software of ESA.</i>
Reference	<i>Chapter 3</i>
<i>Validation Results</i>	
Summary	<i>In RD-6 the PAZ data quality was found to be overall in line with the claimed values given in the PAZ documentation. The intercomparison between PAZ, TSX and CSK performed within this work showed the following results for each of the evaluated quality parameters. Spatial resolution: Very similar spatial resolution for the SM mode of PAZ, TSX and CSK, and for the SL and HS modes of PAZ and TSX. The SC data of PAZ had significantly higher resolution than CSK, but the difference was expected due to different imaging configuration. PSLR and ISLR: The side lobes of PAZ and TSX were very similar in azimuth direction, but the side lobes of PAZ in range direction were systematically 1-7 dB stronger than for TSX in all evaluated imaging modes. For the SC and SM modes, the side lobes of CSK were always stronger compared to PAZ, probably due to different windowing methods used by the data providers. Localization accuracy: The measured localization accuracy of PAZ was overall better than the localization accuracies of TSX and CSK. The precision of the errors for CSK was lower, meaning that the magnitude and direction of the localization errors varied more than for PAZ and TSX. In SM, SL and HS modes, the localization errors of PAZ were typically slightly smaller than for TSX. ENL: The results were similar for PAZ, TSX and CSK. Apart from few outliers, all scenes from the Glacier and the Desert showed ENL close to the ideal values. For the Rainforest site, data of all</i>

	<p>three missions showed values smaller than the ideal ENL, assumably due to target properties not suitable for correct ENL calculation for X-band SAR.</p> <p>NESZ: For the SC, SM and SL single polarization modes the NESZ of PAZ was 0.5-2 dB lower (better) than of the corresponding TSX data, whereas for the SL dual-pol, the NESZ of TSX was more than 4 dB lower than for PAZ. For the HS mode, the NESZ of the TSX single-pol scene was 1 dB lower than of the PAZ dual-pol scene. For the SM mode the NESZ of CSK was somewhat lower and for SC mode significantly lower than the values measured for the corresponding PAZ and TSX data. This large difference can be related to different imaging configuration of CSK compared to PAZ and TSX. Nevertheless, the measured NESZ for the PAZ, TSX, and CSK data were all generally in line with the specifications provided in the product documents.</p> <p>AEP: The AEP correction applied in PAZ was more successful compared to TSX and CSK for the SC mode and compared to TSX for the SL and HS modes. For the SM mode, PAZ and TSX showed correct patterns in all acquisitions, while half of the CSK scenes showed decreasing normalized backscatter trend in the far range.</p>
Reference	<p>RD-2 Chapter 3</p>

3. DETAILED ASSESSMENT

This chapter provides detailed information on the independent data analysis and intercomparison performed by FMI for the PAZ, TSX and CSK satellite data products. Table 2 shows the date, acquisition mode, polarization, processing mode and version number of the PAZ scenes provided by Hisdesat and used by the evaluation team for the assessment and comparison with TSX and CSK within the EDAP activity. Table 3 and Table 4 show the same information for the TSX and CSK data products used in the intercomparison. Data were collected from various test sites enabling a comprehensive assessment of the most relevant SAR quality metrics, such as spatial resolution, PSLR, ISLR, geolocation accuracy, ENL, NESZ and AEP.

The first part of the PAZ data was delivered to FMI in May 2020. The version of these data is 1.2. Additional data from the corner reflector sites of Neustrelitz in Germany and Rosamond in California, were ordered later, and delivered to FMI during the first half of 2021. The version of these data is 1.6. The first part of the TSX data was delivered to FMI during August-October 2021, and the second part during December 2021 and January 2022. All CSK data was delivered to FMI in August 2021. PAZ and TSX data included archive scenes acquired previously by the satellites as well as new acquisitions ordered specifically for the purpose of the EDAP evaluation. The CSK data products were all archive scenes. PAZ, TSX and CSK data were ordered for the same, or at least similar test areas and imaging modes, and with as similar imaging properties as possible, such as incidence angle and polarization. The analysed PAZ and TSX data included SC, SM, SL and HS products, whereas CSK data included only SM and SC products.

The data used for assessment includes scenes from distributed homogeneous and low backscatter areas, as well as point target test sites with corner reflectors. The homogeneous targets are used for evaluating the ENL and the AEP. The homogeneous test areas include scenes from the Amazonas Rainforest and Antarctica Glacier. Low backscatter targets are used for assessing the NESZ. Low backscatter scenes were acquired from the Pacific Ocean, Michigan Lake USA, and from the Sahara Desert. The corner reflector test sites used are from Neustrelitz in Germany and Rosamond in California. An IRF analysis is performed over the corner reflectors, providing quality values for spatial resolution, geolocation accuracy, and the power distribution of the measured radar beam (PSLR and ISLR).

The SAR Quality Toolbox provided by Aresys was used for assessing the above-mentioned metrics. The quality values measured from the PAZ data were compared with the corresponding quality values measured from the TSX and the CSK satellite data products.

Table 2: All PAZ data products provided by Hisdesat to FMI and included in the data analysis and evaluation.

Test Area	Date	Acquisition mode	Polarization	Processing mode	Version number
Desert, Sahara	20180924	SL	HH / HV	SSC	1.2
	20180913	SL	HH	SSC	1.2
	20181111	SM	VV	SSC	1.2
	20181122	SM	VV	SSC	1.2
Rosamond, California	20210206	SC	HH	MGD	1.6
	20210217	SC	HH	MGD	1.6
	20210228	SC	VV	MGD	1.6
	20210311	SC	VV	MGD	1.6
Neustrelitz, Germany	20200712	HS	HH	SSC	1.2
	20200717	HS	HH	SSC	1.2
	20201229	HS	VV	SSC	1.6
	20210131	HS	VV	SSC	1.6
	20210316	SL	HH	SSC	1.6
	20210327	SL	HH	SSC	1.6
	20210407	SL	VV	SSC	1.6
	20210418	SL	VV	SSC	1.6

	20200329	SM	VV	SSC	1.2
	20200409	SM	HH	SSC	1.2
	20200420	SM	VV	SSC	1.2
	20200501	SM	HH	SSC	1.2
Glacier, Antarctica	20190303	SC	VV	MGD	1.2
	20190423	SC	HH	MGD	1.2
	20180928	SM	VV	SSC	1.2
	20180930	SM	VV	SSC	1.2
Low backscatter, water surfaces	20181025	SC	HH	MGD	1.2
	20181026	HS	HH / HV	SSC	1.2
	20181027	SM	HH / HV	SSC	1.2
	20181025	SM	HV	SSC	1.2
Rainforest, Amazon	20180724	SC	HH	MGD	1.2
	20180917	HS	VV	SSC	1.2
	20180917	SL	HH / VV	SSC	1.2
	20180729	SM	VV	SSC	1.2
	20180829	SM	VV	SSC	1.2
	20190111	SM	HH	SSC	1.2

Table 3: All TSX data products provided by Airbus to FMI and included in the data analysis and evaluation.

Test Area	Date	Acquisition mode	Polarization	Processing mode	Version number
Desert, Sahara	20071119	SL	HH	SSC	4.11
	20080820	SL	HH	SSC	4.11
	20100718	SL	HH / VV	SSC	4.11
	20100513	SM	VV / VH	SSC	4.11
	20100513	SM	VV / VH	SSC	4.11
	20100907	SM	VV / VH	SSC	4.11
	20101021	SM	VV / VH	SSC	4.11
Rosamond, California	20180804	SC	HH	MGD	4.11
	20211002	SC	HH	MGD	4.11
	20211013	SC	VV	MGD	4.11
	20220109	SC	VV	MGD	4.11
Neustrelitz, Germany	20200405	SM	HH	SSC	4.11
	20200508	SM	HH	SSC	4.11
	20200610	SM	HH	SSC	4.11
	20201214	SM	VV	SSC	4.11
	20210116	SM	VV	SSC	4.11
	20210218	SM	VV	SSC	4.11
	20210722	SL	HH	SSC	4.11
	20210802	SL	HH	SSC	4.11
	20210824	HS	HH	SSC	4.11
	20210904	SL	VV	SSC	4.11
	20211201	SL	VV	SSC	4.11
	20211212	HS	HH	SSC	4.11
	20211223	HS	VV	SSC	4.11
	20220103	HS	VV	SSC	4.11
Glacier, Antarctica	20100512	SC	VV	MGD	4.11
	20150708	SC	HH	MGD	4.11
	20150708	SC	HH	MGD	4.11
	20071212	SM	VV / VH	SSC	4.11
	20100310	SM	HH / VV	SSC	4.11
	20200410	SM	VV / VH	SSC	4.11
	20100426	SM	VV	SSC	4.11
	20190718	SM	VV	SSC	4.11
Low backscatter, water surfaces	20111211	HS	HH	SSC	4.11
	20200815	SC	HH	MGD	4.11
	20160507	SM	HH / VV	SSC	4.11
	20180815	SM	HH	SSC	4.11

Rainforest, Amazon	20140923	SL	HH	SSC	4.11
	20141017	SM	HH	SSC	4.11
	20170930	SC	HH	MGD	4.11
	20140804	SM	HH / VV	SSC	4.11
	20140727	SM	HH / VV	SSC	4.11
	20150318	SM	VV	SSC	4.11
	20140121	SM	HH	SSC	4.11
	20160329	SL	VV	SSC	4.11
	20100718	SL	HH / VV	SSC	4.11
	20101130	HS	HH / VV	SSC	4.11
	20090323	HS	HH / VV	SSC	4.11
	20171103	SC	HH	MGD	4.11

Table 4: All Cosmo-SkyMed data products provided by e-GEOS to FMI and included in the data analysis and evaluation.

Test Area	Date	Acquisition mode	Polarization	Processing mode	L1A Software Version
Desert, Sahara	20170401	HI	VV	SSC	01.04.24
	20170430	HI	VV	SSC	01.04.24
	20170409	HI	VV	SSC	01.04.24
Rosamond, California	20130401	WR	VV	DGM	4.0.12
	20130321	WR	VV	DGM	4.0.12
	20130411	WR	VV	DGM	4.0.12
	20140627	WR	HH	DGM	4.0.12
	20130327	WR	HH	DGM	4.0.12
Neustrelitz, Germany	20190704	HI	HH	SSC	01.04.24
	20190523	HI	HH	SSC	01.04.24
	20190416	HI	HH	SSC	01.04.24
	20190720	HI	VV	SSC	01.04.24
	20160412	HI	VV	SSC	01.04.24
	20160127	HI	VV	SSC	01.04.24
Glacier, Antarctica	20130507	HR	HH	DGM	4.0.12
	20090611	HR	HH	DGM	4.0.12
	20090817	HR	VV	DGM	4.0.12
	20090817	HR	VV	DGM	4.0.12
	20111214	HI	VV	SSC	01.04.24
	20111222	HI	VV	SSC	01.04.24
	20130704	HI	VV	SSC	01.04.24
	20130727	HI	VV	SSC	01.04.24
Low backscatter, water surfaces	20090602	WR	HH	DGM	4.0.12
	20160726	WR	HH	DGM	4.0.12
	20150427	HI	HH	SSC	01.04.24
	20150428	HI	HH	SSC	01.04.24
Rainforest, Amazon	20170701	WR	HH	DGM	4.0.12
	20090217	HI	VV	SSC	01.04.24
	20090226	HI	VV	SSC	01.04.24
	20150120	HI	VV	SSC	01.04.24
	20191130	HI	VV	SSC	01.04.24
	20170324	WR	HH	DGM	4.0.12
	20180319	HI	HH	SSC	01.04.24
20191126	HI	HH	SSC	01.04.24	

3.1 IRF Analysis

The PAZ, TSX and CSK data for the IRF analysis of this work have been acquired over two test sites: Neustrelitz in Germany and Rosamond in California, USA. The Neustrelitz site was used for assessing the higher spatial resolution HS, SL and SM data, whereas the Rosamond site was used

for the SC data assessment. The analysis in Neustrelitz included all relevant aspects of the IRF-assessment, including geolocation accuracy assessment. It was not possible to perform the IRF analysis for the TSX SC MGD data in the SQT, because the product was not yet supported by the software. Therefore, for the SC mode, only a localization accuracy assessment comparing TSX and PAZ data was conducted using the SNAP toolbox, without assessing the spatial resolution and the side lobes of the TSX SC data. Nevertheless, a complete IRF analysis was conducted for PAZ and CSK SC data over Rosamond.

Figure 1 shows a Google Earth view of the Neustrelitz site. The site contains 4 trihedral corner reflectors with a face width of 1.5 m. Three of the reflectors; D33, D35 and D36, are directed to the west (ascending right looking orbits) and were therefore visible in the acquired PAZ, TSX and CSK scenes. The coordinates of the Neustrelitz CR locations are presented in Table 5.

Table 5: Coordinates of the Neustrelitz corner reflectors.

CR name	Latitude (decimal degrees)	Longitude (decimal degrees)	Elevation (metres above sea level)
D33	53.32945	13.06939	67
D34	53.33008	13.06963	70
D35	53.33020	13.06952	70
D36	53.32938	13.06991	65

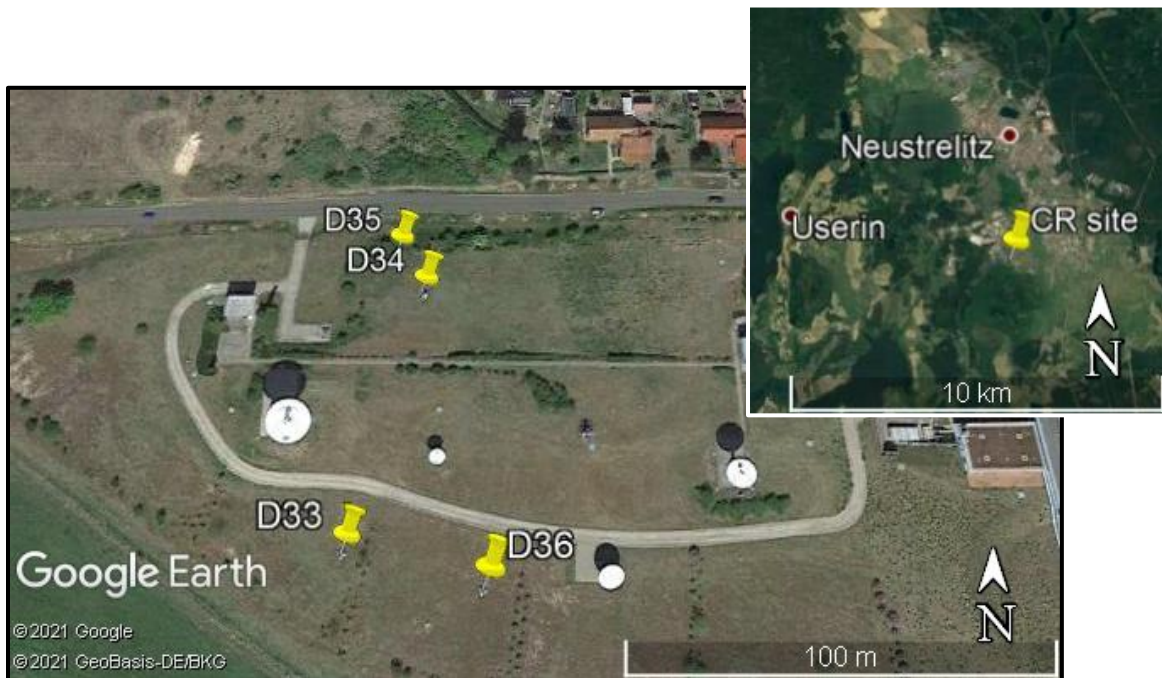


Figure 1: A Google Earth view of the Neustrelitz corner reflector (CR) site in Germany. The small image in the upper right side is a zoom out showing the surrounding area of the CR site. The large image is a zoom in on the CR site, showing the CR names and distribution at the site.

Figure 2 shows a Google Earth view of the Rosamond site maintained by NASA's Jet Propulsion Laboratory. The Rosamond site contains several trihedral CRs with face widths of 4.8 m, 2.4 m, and 0.7 m. Most of the reflectors are directed towards the east (descending right looking orbits), including all large (4.8 m), all small (0.7 m) and part of the medium size (2.4 m) reflectors, thus they are visible in the acquired PAZ, TSX and CSK scenes. The coordinates of the CR locations in the

Rosamond calibration site are publicly available through the NASA JPL website: <https://uavsar.jpl.nasa.gov/cgi-bin/calibration.pl>.

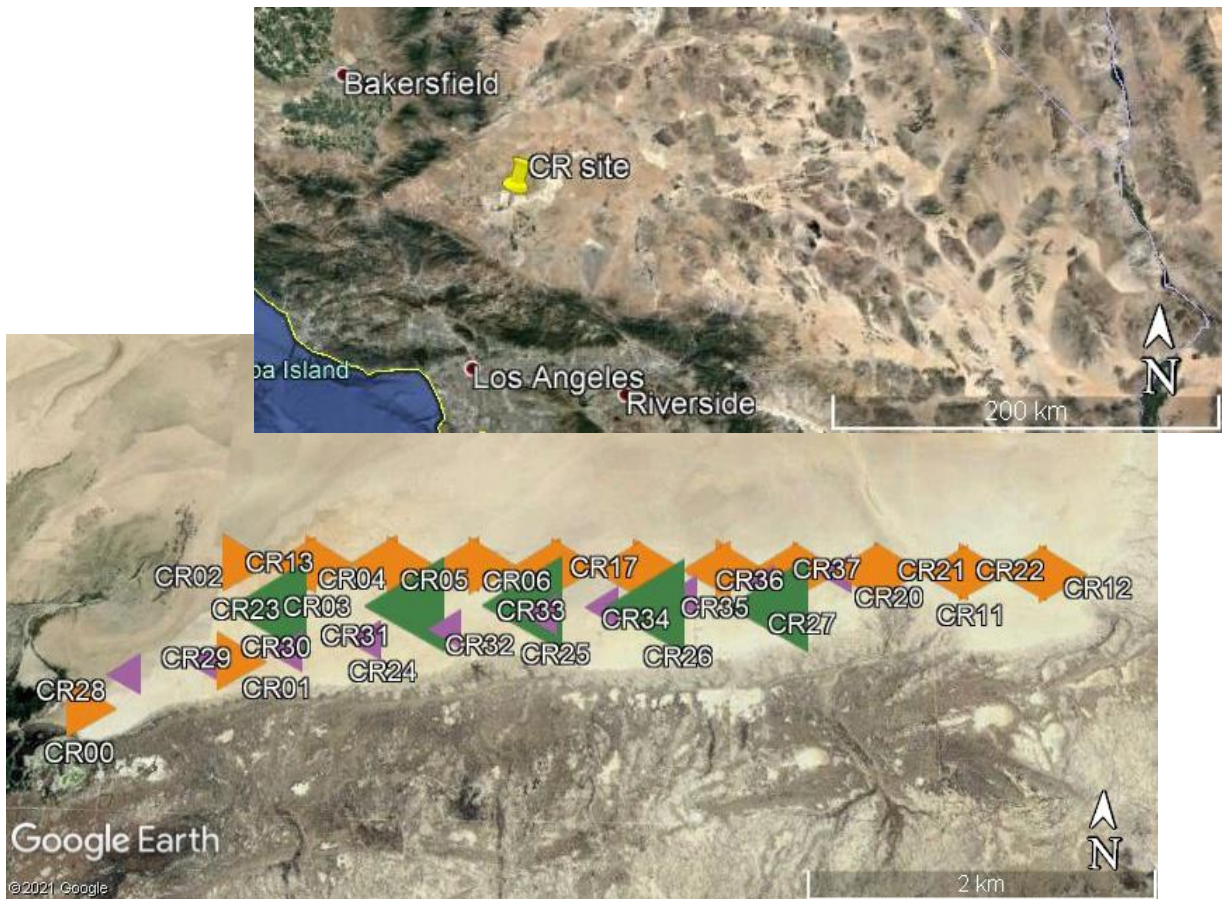


Figure 2: A Google Earth view of the Rosamond CR site in California. The smaller image in the upper right side is a zoom out showing the surrounding area of the CR site. The bottom image is a zoom in on the CR site, showing the CR names, alignment, and distribution at the site.

The IRF-analysis is performed using the SQT software of Aresys. A screenshot showing an example of an IRF-analysis in the SQT for Neustrelitz is shown in Figure 3. The red points over the PAZ SAR image show the location of the reflectors.

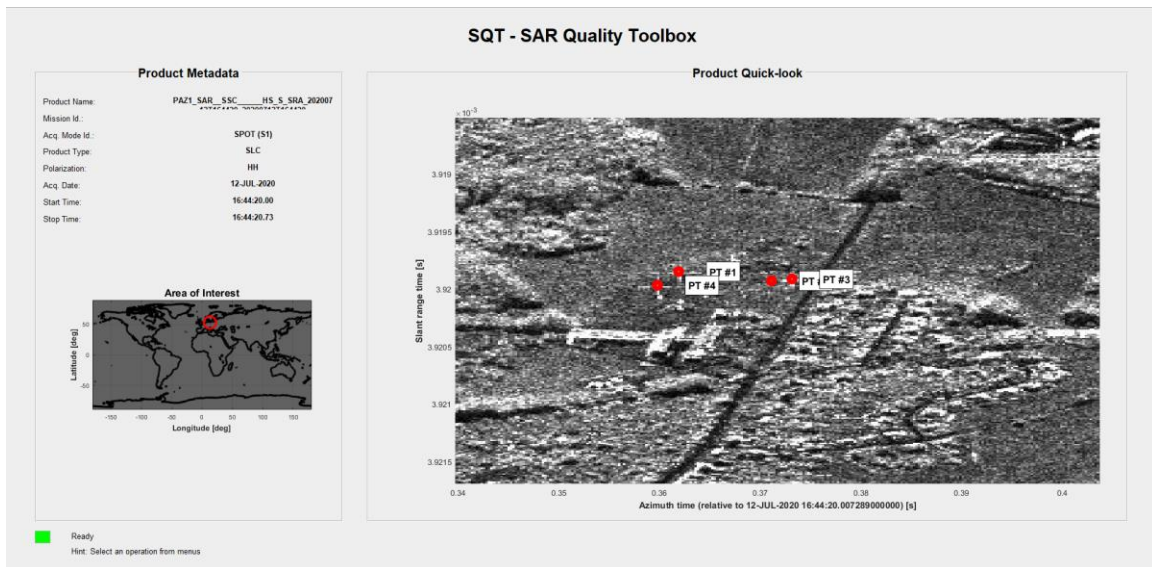


Figure 3: IRF-analysis in Neustrelitz, Germany, using the SQT. The red points show the location of the corner reflectors over a PAZ HS image.

The IRF-analysis typically includes an indication of the localization error of a SAR scene. The given locations of the bright targets (corner reflectors) are compared with the locations of the reflectors in the SAR image. The localization error is expressed in both azimuth and range directions. Figure 4 shows an example of the localization error based on one specific corner reflector. The red dot is the expected location of the reflector on the SAR image, based on the geographical coordinates of the reflector (e.g. the true location). The green plus (+) sign shows the location of the same reflector on the SAR image, calculated by the software based on the backscatter distribution.

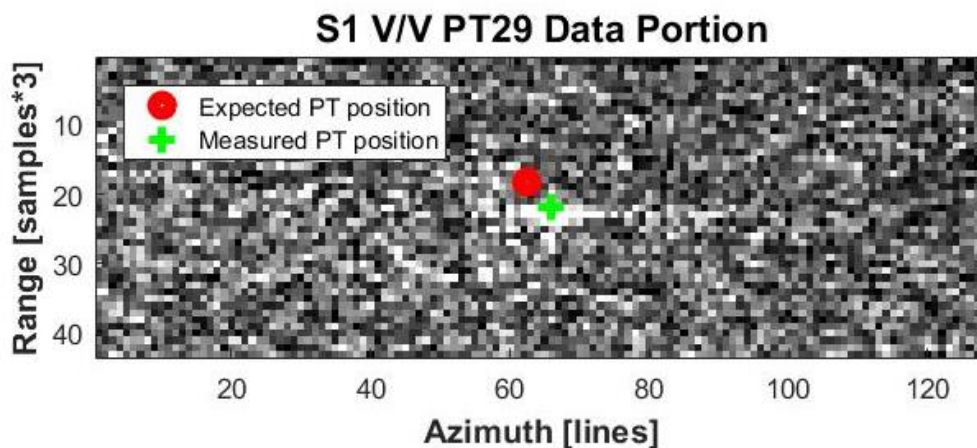


Figure 4: Geolocation accuracy assessment with the SQT. The expected point target (red dot) location is compared with the location in the observed SAR image (green plus sign).

The distribution of the measured power from the reflectors and the area around the reflectors are analysed, providing the spatial resolution of the SAR data and the power of the secondary lobes relative to the main lobe (PSLR and ISLR). Figure 5 shows an example of the spatial distribution of the measured power over one of the corner reflectors seen in a PAZ HS image.

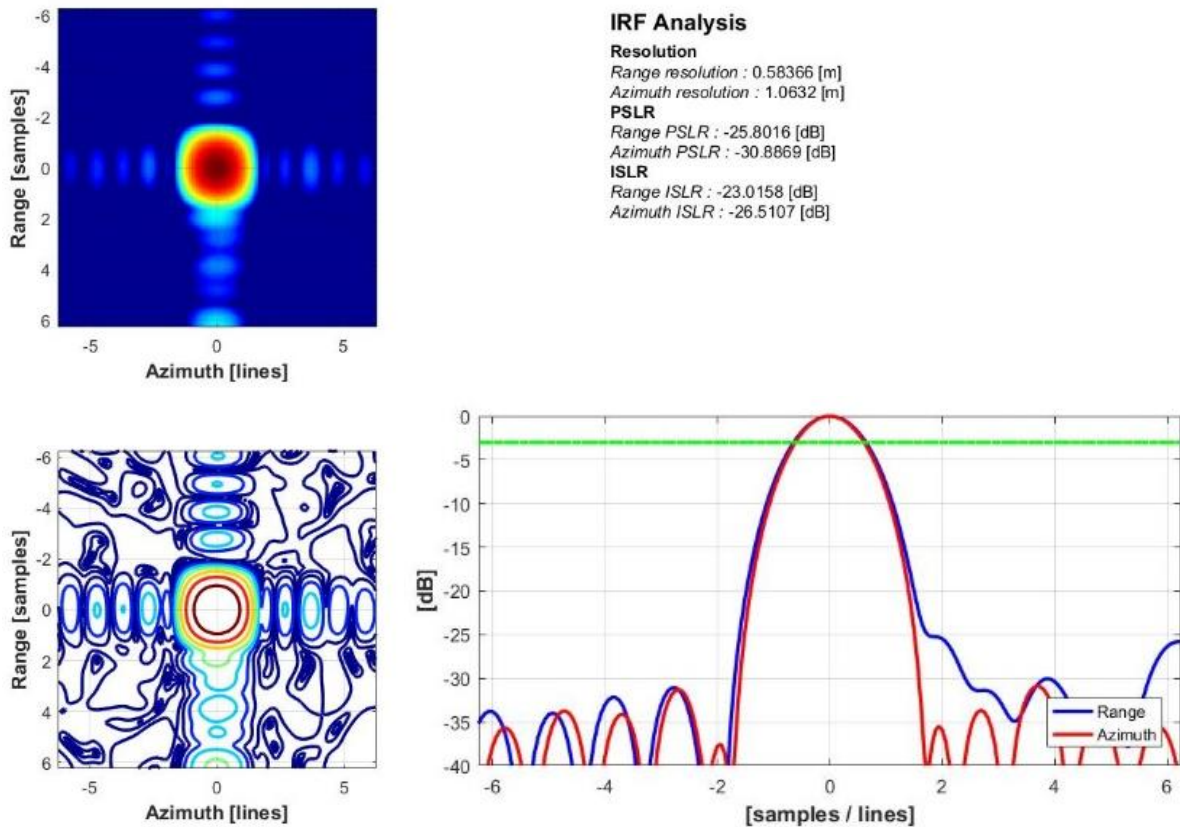


Figure 5. Example of an IRF analysis of a PAZ HS scene with the SQT over one CR.

The products are assessed by intercomparing the measured IRF parameter values of the different satellite data providers; PAZ, TSX and CSK. As an additional reference, Table 6, Table 7 and Table 8 show the IRF-values provided in the PAZ, TSX and CSK documentation, respectively. The range spatial resolution is given in slant range direction for SSC/SCS, and ground range direction for MGD/DGM products. For PAZ, PSLR and ISLR values have not been directly provided by Hisdesat, but the used alpha coefficient in the applied Hamming window filter was given; $\alpha = 0.6$. A geolocation uncertainty of 2 m for the standard products due to the accuracy of the GPS orbit determination is reported in the PAZ documentation.

Table 6: Quality values of the PAZ single-pol test datasets related to the IRF-analysis, provided in the PAZ documentation. The theoretical PSLR and ISLR values correspond to the alpha coefficient 0.6 used in the Hamming windowing. The 1-sigma localization error of the standard product is provided.

Product type	Range resolution [m]	Azimuth resolution [m]	Localization error [m]	Theoretical PSLR [dB] ($\alpha = 0.6$)	Theoretical ISLR [dB] ($\alpha = 0.6$)
ScanSAR MGD	16.79 - 18.19 (45°...20°)	17.66 - 18.18 (45°...20°)	2	-31.60	-26.18
Stripmap SSC	1.76 (100 MHz)	3.01	2	-31.60	-26.18
Spotlight SSC	1.18	1.46	2	-31.60	-26.18
HR Spotlight SSC	0.6	1.05	2	-31.60	-26.18

Table 7 shows the IRF quality values reported in the TSX documentation. Due to the similarity of PAZ and TSX, the TSX quality values are close to the values reported for PAZ. The specified nominal localization accuracy of the TSX standard products is 2 m. However, depending on the actual conditions in the media (vacuum, ionosphere and troposphere) passed by the signal and on the incidence angle, a localization error of 2-4 m is expected. Table 8 shows the IRF quality values reported in the CSK documentation for the analysed imaging modes.

Table 7: Quality values of the TSX single polarization test datasets related to the IRF-analysis, provided in the TSX documentation. The 1-sigma localization error of the standard product is provided.

Product type	Range resolution [m]	Azimuth resolution [m]	Localization error [m]	PSLR [dB]	ISLR [dB]
ScanSAR MGD	17 - 19.2 (45°...20°)	18.5 - 19.2 (45°...20°)	2 - 4	Not specified	Not specified
Stripmap SSC	1.2	3.3	2 - 4	-25	-18
Spotlight SSC	1.2	1.7	2 - 4	-25	-18
HR Spotlight SSC	0.6	1.1	2 - 4	-25	-18

Table 8: Quality values of the CSK test datasets related to IRF-analysis, provided in the CSK documentation. The 3-sigma localization error is provided.

Product type	Range resolution [m]	Azimuth resolution [m]	Localization error [m]	PSLR [dB]	ISLR [dB]
ScanSAR WR MGD	30	30	9.23	-22	-12
Stripmap HI SSC	2.6 - 3	2.4 - 2.6	11.19	-22	-12

3.1.1 PAZ

Table 9 and Table 10 show the IRF quality values measured for the PAZ data in Rosamond and Neustrelitz, respectively. The measured range and azimuth resolutions of the single-pol SC data over Rosamond were very similar in all four images. The range resolution was close to 16.6 m and the azimuth resolution was close to 19.2. The measured localization errors were ~4.1 m in range and ~-3.3 m in azimuth directions. The PSLR in range and azimuth directions were around -23 dB and -27 dB, and the ISLR in range and azimuth around -18 dB and -21 dB, respectively.

Table 9: IRF-analysis results of the PAZ SC scenes from Rosamond, California; ground range and azimuth resolution, PSLR and ISLR, as well as localization error. The table shows the average values calculated from all corner reflectors.

Scene	Range resolution [m]	Azimuth resolution [m]	Range PSLR [dB]	Azimuth PSLR [dB]	Range ISLR [dB]	Azimuth ISLR [dB]	Range Location Error [m]	Azimuth Location Error [m]
SC_20210206T135845	16.634 ± 0.035	19.13 ± 0.135	-23.458 ± 1.486	-26.711 ± 1.578	-18.318 ± 1.259	-21.351 ± 2.457	4.053 ± 0.066	-3.311 ± 0.131
SC_20210217T135844	16.621 ± 0.037	19.198 ± 0.151	-23.423 ± 1.208	-27.415 ± 3.181	-18.102 ± 2.182	-22.072 ± 3.991	4.003 ± 0.058	-3.297 ± 0.088
SC_20210228T135844	16.64 ± 0.035	19.183 ± 0.122	-23.325 ± 2.352	-27.057 ± 4.106	-17.758 ± 3.062	-21.238 ± 4.621	4.142 ± 0.051	-3.372 ± 0.095
SC_20210311T135844	16.625 ± 0.045	19.168 ± 0.209	-23.728 ± 2.341	-25.792 ± 2.743	-17.88 ± 2.316	-19.785 ± 3.253	4.108 ± 0.038	-3.178 ± 0.489

The measured slant range resolution in the Neustrelitz scenes were typically 0.6 m in HS, 1.17 m in SL and 1.75 m in SM. The measured azimuth resolution in Neustrelitz was typically 1.1 m for HS, 1.6 m for SL and 3.0 m for SM. The derived range and azimuth localization errors for Neustrelitz scenes were around 2.5 m and 0.2 m for HS, 2.7 m and 0.3 m for SL, and 2.6 m and 0.2 m for SM, respectively. The PSLR in range and azimuth directions were around -24 dB and -30 dB for HS, -25 dB and -30 dB for SL, and -26 dB and -30 dB for SM, respectively. The derived ISLR in range and azimuth direction were -22 dB and -25 dB for HS, -23 dB and -25 dB for SL, and -24 dB and -25 dB for SM acquisition mode, respectively.

Table 10: IRF-analysis results of the PAZ SM, SL and HS scenes from Neustrelitz, Germany; ground range and azimuth resolution, PSLR and ISLR, as well as localization error. The table shows the average values calculated from all CRs.

Scene	Range resolution [m]	Azimuth resolution [m]	Range PSLR [dB]	Azimuth PSLR [dB]	Range ISLR [dB]	Azimuth ISLR [dB]	Range Location Error [m]	Azimuth Location Error [m]
HS_20200712T164420	0.583 ± 0.001	1.067 ± 0.001	-25.827 ± 0.116	-30.767 ± 0.468	-22.543 ± 0.509	-25.347 ± 0.085	2.045 ± 0.241	0.111 ± 0.124
HS_20200717T165253	0.659 ± 0.101	1.157 ± 0.16	-23.591 ± 2.217	-28.424 ± 1.382	-21.079 ± 2.238	-24.596 ± 1.876	2.845 ± 0.228	0.143 ± 0.165
HS_20201229T165256	0.629 ± 0.039	1.12 ± 0.09	-24.331 ± 1.526	-30.445 ± 1.461	-21.291 ± 1.149	-24.986 ± 0.638	2.566 ± 0.227	0.184 ± 0.18
HS_20210109T165256	0.604 ± 0.011	1.11 ± 0.025	-24.011 ± 1.108	-31.464 ± 1.66	-21.64 ± 1.053	-25.638 ± 0.129	2.729 ± 0.2	0.34 ± 0.133
SL_20210316T165254	1.17 ± 0.001	1.555 ± 0.002	-25.307 ± 0.117	-29.781 ± 0.577	-23.19 ± 0.09	-25.359 ± 0.242	2.668 ± 0.198	0.263 ± 0.124
SL_20210327T165254	1.17 ± 0.001	1.563 ± 0.003	-25.6 ± 0.638	-30.125 ± 0.635	-23.931 ± 1.387	-25.429 ± 0.232	2.797 ± 0.201	0.264 ± 0.124
SL_20210407T165255	1.168 ± 0.001	1.561 ± 0.002	-25.256 ± 0.572	-29.516 ± 0.298	-23.204 ± 0.18	-25.264 ± 0.329	2.67 ± 0.198	0.207 ± 0.135
SL_20210418T165256	1.167 ± 0.002	1.551 ± 0.001	-25.238 ± 0.282	-29.656 ± 0.58	-23.207 ± 0.053	-25.359 ± 0.137	2.635 ± 0.196	0.25 ± 0.134
SM_20200329T165246	1.748 ± 0.004	2.958 ± 0.004	-26.104 ± 0.324	-30.568 ± 0.544	-24.808 ± 0.232	-25.051 ± 0.723	2.605 ± 0.19	0.23 ± 0.132
SM_20200409T165247	1.753 ± 0.005	2.952 ± 0.022	-26.227 ± 0.267	-30.237 ± 0.836	-24.801 ± 0.036	-25.347 ± 0.385	2.719 ± 0.192	0.244 ± 0.109
SM_20200420T165248	1.75 ± 0.003	2.962 ± 0.004	-26.716 ± 0.594	-30.642 ± 0.954	-24.122 ± 1.911	-25.135 ± 0.758	2.734 ± 0.193	0.225 ± 0.136
SM_20200501T165248	1.752 ± 0.004	2.966 ± 0.005	-26.661 ± 0.536	-29.764 ± 0.719	-23.991 ± 1.325	-25.16 ± 0.431	2.574 ± 0.189	0.176 ± 0.097

3.1.2 TSX

The TSX SC data from Rosamond could not be processed in the SQT, because the product was not yet supported by the software. Therefore, a proper IRF analysis including an assessment of the spatial resolution and the side lobes was not possible. Nevertheless, a localization error assessment was performed for the TSX SC data in the SNAP software. For a better comparison with PAZ, the same localization error analysis in SNAP was also done for the PAZ SC data from Rosamond. Table 11 shows the localization error measured for the TSX and PAZ SC data over Rosamond. The average distance between the location of the CRs on the SAR images and their coordinates is given in x- and y-axis, namely in West-East and South-North directions, respectively. The average and the standard deviation of the Absolute Localization Error (ALE) are also given. The averages and the standard deviations were calculated from all available CRs over the test area.

The measured localization error of the TSX data in x-axis was close to 19 m, and in y-axis close to -4 m. The CRs in the TSX SAR images were thus approximately 19 m east and 4 m south from their true location, corresponding to an ALE between 19 and 20 m, with a standard deviation of less than 1.3 m between the ALE of the different CRs. The measured localization errors for PAZ were close to 10 m and -2 m in x- and y-axis, respectively. The CRs in the PAZ images were thus approximately 10 m east and 2 m south from their true location, corresponding to an ALE between 10 and 11 m, with a standard deviation of less than 1 m between the ALE of the different CRs.

Table 11: Average geolocation errors of the TSX and PAZ SC scenes, in West-East (dx) and South-North (dy) directions, as well as the average absolute location error (ALE) and the standard deviation (STD) of the ALE for the CR's over the Rosamond site.

Scene (sensor and date)	Average dx	Average dy	Average ALE	STD ALE
TSX 20180804	19.16	-3.95	19.58	1.27
TSX 20211002	18.66	-3.71	19.05	1.32
TSX 20211013	19.43	-3.97	19.85	1.01
TSX 20220109	19.50	-3.86	19.90	0.98
PAZ 20210206	10.15	-2.15	10.40	0.78
PAZ 20210217	10.20	-1.91	10.40	0.94
PAZ 20210228	10.47	-1.94	10.67	0.98
PAZ 20210311	10.33	-2.15	10.58	0.73

Table 12 shows the IRF quality values measured for the TSX data in Neustrelitz, Germany. The measured slant range resolution in the Neustrelitz scenes was typically 0.62 m in HS, 1.18 m in SL and 1.76 m in SM imaging mode. The measured azimuth resolution in Neustrelitz was typically 1.08 m for HS, 1.57 m for SL and 2.96 m for SM. The derived range and azimuth localization errors for the TSX Neustrelitz scenes were typically around 2.8 m and 0.2 m for HS, 2.8 m and 0.2 m for SL, and 2.7 m and 0.2 m for SM, respectively. The PSLR in range and azimuth directions were around -31 dB and -30 dB for HS, -28 dB and -30 dB for SL, and -29 dB and -30 dB for SM, respectively. The derived ISLR in range and azimuth directions were typically -26 dB for HS, -25 dB for SL, and -25 dB for SM acquisition mode.

Table 12: IRF-analysis results of the TSX SM, SL and HS scenes from Neustrelitz, Germany; ground range and azimuth resolution, PSLR and ISLR, as well as localization error. The table shows the average values calculated from all CRs.

Scene	Range resolution [m]	Azimuth resolution [m]	Range PSLR [dB]	Azimuth PSLR [dB]	Range ISLR [dB]	Azimuth ISLR [dB]	Range Location Error [m]	Azimuth Location Error [m]
HS_20211212T165401	0.603 ± 0.007	1.071 ± 0.009	-31.836 ± 0.264	-30.303 ± 0.281	-26.623 ± 0.195	-25.32 ± 0.08	2.817 ± 0.202	0.193 ± 0.115
HS_20211223T165400	0.607 ± 0.007	1.062 ± 0.004	-31.088 ± 0.367	-30.16 ± 0.386	-26.168 ± 0.328	-25.951 ± 0.744	2.736 ± 0.191	0.285 ± 0.13
HS_20220103T165359	0.624 ± 0.021	1.096 ± 0.038	-30.296 ± 0.721	-30.741 ± 1.42	-25.849 ± 0.755	-26.25 ± 0.914	2.798 ± 0.196	0.259 ± 0.122
HS_20210824T165400	0.648 ± 0.042	1.089 ± 0.036	-29.713 ± 1.97	-29.831 ± 0.231	-24.727 ± 1.343	-26.026 ± 1.08	2.911 ± 0.246	0.187 ± 0.177
SL_20210722T165358	1.178 ± 0.002	1.57 ± 0.005	-27.353 ± 0.514	-30.376 ± 0.411	-24.895 ± 0.187	-25.353 ± 0.54	2.912 ± 0.193	0.237 ± 0.105
SL_20210904T165400	1.181 ± 0.001	1.565 ± 0.005	-28.292 ± 0.202	-30.686 ± 0.353	-25.226 ± 0.05	-25.417 ± 0.23	2.845 ± 0.205	0.255 ± 0.129
SL_20211201T165401	1.179 ± 0.001	1.566 ± 0.003	-27.836 ± 0.924	-30.516 ± 0.371	-25.043 ± 0.113	-25.428 ± 0.228	2.637 ± 0.206	0.201 ± 0.123

SL_20210802T165358	1.179 ± 0.003	1.565 ± 0.001	-27.895 ± 0.202	-30.301 ± 0.284	-34.074 ± 15.658	-25.313 ± 0.16	2.88 ± 0.199	0.182 ± 0.107
SM_20200405T165344	1.767 ± 0.003	2.973 ± 0.021	-26.807 ± 5.325	-30.511 ± 1.129	-24.777 ± 0.843	-25.509 ± 0.192	2.8 ± 0.191	0.203 ± 0.128
SM_20200508T165345	1.764 ± 0.003	2.967 ± 0.006	-29.585 ± 0.788	-30.484 ± 0.335	-24.032 ± 1.694	-25.162 ± 0.507	2.74 ± 0.191	0.232 ± 0.144
SM_20200610T165348	1.765 ± 0.003	2.962 ± 0.001	-29.841 ± 0.523	-30.74 ± 0.657	-24.2 ± 1.598	-25.294 ± 0.334	2.759 ± 0.195	0.192 ± 0.134
SM_20201214T165353	1.767 ± 0.001	2.962 ± 0.002	-29.21 ± 0.724	-30.481 ± 0.315	-24.849 ± 0.265	-25.45 ± 0.46	2.832 ± 0.199	0.277 ± 0.11
SM_20210116T165351	1.764 ± 0.001	2.966 ± 0.002	-30.405 ± 0.584	-30.354 ± 0.57	-24.906 ± 0.087	-25.427 ± 0.258	2.724 ± 0.201	0.192 ± 0.115
SM_20210218T165349	1.761 ± 0.001	2.964 ± 0.003	-29.757 ± 0.511	-30.434 ± 0.84	-24.747 ± 0.386	-24.907 ± 0.756	2.63 ± 0.201	0.195 ± 0.135

3.1.3 CSK

Table 13 shows the IRF quality values measured for the CSK SC WR data in Rosamond. The measured spatial resolution in range and azimuth directions was close to 29 m. The measured localization errors were between -6.2 and 8.4 m in range, and between -1.6 and 0.5 m in azimuth direction. The PSLR in range and azimuth directions were between -15 and -22 dB, and the ISLR in range and azimuth between -8 and -17 dB.

Table 13: IRF-analysis results of the CSK SC WR scenes from Rosamond, California; ground range and azimuth resolution, PSLR and ISLR, as well as localization error. The table shows the average values calculated from all corner reflectors.

Scene	Range resolution [m]	Azimuth resolution [m]	Range PSLR [dB]	Azimuth PSLR [dB]	Range ISLR [dB]	Azimuth ISLR [dB]	Range Location Error [m]	Azimuth Location Error [m]
WR_20130401015326	27.411 ± 0.249	29.64 ± 0.102	-18.228 ± 1.625	-20.914 ± 3.453	-11.914 ± 1.841	-14.608 ± 3.932	-0.634 ± 1.481	-0.696 ± 0.243
WR_20130321014729	29.372 ± 0.148	29.204 ± 0.102	-20.827 ± 1.318	-22.183 ± 0.652	-15.886 ± 1.42	-14.973 ± 1.822	1.956 ± 2.091	-1.389 ± 0.438
WR_20130411014119	29.571 ± 0.034	29.027 ± 0.074	-21.744 ± 0.191	-21.729 ± 0.314	-16.947 ± 0.135	-16.116 ± 0.161	8.393 ± 1.122	0.481 ± 0.436
WR_20140627015046	28.947 ± 0.71	29.909 ± 0.645	-15.383 ± 1.842	-16.853 ± 0.54	-7.81 ± 1.285	-9.01 ± 0.578	-6.205 ± 1.044	-1.566 ± 0.542
WR_20130327014126	29.717 ± 0.05	29.062 ± 0.073	-21.819 ± 0.834	-21.523 ± 0.963	-17.278 ± 0.229	-12.948 ± 3.943	8.173 ± 1.263	-0.686 ± 0.112

Table 14 shows the IRF quality values measured for the CSK SM HI data in Neustrelitz. The measured slant range resolution in the Neustrelitz scenes varied between 1.4 and 2.2 m, and the measured azimuth resolution between 2.7 and 2.9 m. The derived range and azimuth localization errors were between -0.9 and 2.9 m, and between -2.4 and -1.4 m, respectively. The measured PSLR in range direction was between -22 and -25 dB and in azimuth direction around -27 dB. The ISLR in range direction was between -19 and -20, and in azimuth direction between -21 and -24 dB.

Table 14: IRF-analysis results of the CSK SM HI scenes from Neustrelitz, Germany; ground range and azimuth resolution, PSLR and ISLR, as well as localization error. The table shows the average values calculated from all CRs.

Scene	Range resolution [m]	Azimuth resolution [m]	Range PSLR [dB]	Azimuth PSLR [dB]	Range ISLR [dB]	Azimuth ISLR [dB]	Range Location Error [m]	Azimuth Location Error [m]
HI_20190704043057	1.367 ± 0.007	2.945 ± 0.013	-23.461 ± 0.806	-26.372 ± 0.567	-19.665 ± 0.006	-21.882 ± 0.155	-0.851 ± 0.243	-2.358 ± 0.149
HI_20190523044257	1.905 ± 0.002	2.745 ± 0.005	-21.9 ± 0.165	-27.255 ± 1.224	-18.703 ± 0.129	-23.395 ± 0.317	0.587 ± 0.173	-2.114 ± 0.156
HI_20190416044856	2.235 ± 0.006	2.742 ± 0.01	-22.509 ± 0.267	-26.78 ± 0.652	-19.021 ± 0.072	-23.054 ± 0.372	0.072 ± 0.148	-1.746 ± 0.161
HI_20190720043058	1.366 ± 0.003	2.932 ± 0.002	-23.594 ± 0.477	-25.563 ± 0.782	-19.776 ± 0.187	-20.909 ± 0.189	-0.783 ± 0.246	-2.111 ± 0.149
HI_20160412044433	1.899 ± 0.001	2.753 ± 0.004	-23.178 ± 0.472	-27.623 ± 0.683	-19.4 ± 0.069	-23.555 ± 0.119	0.482 ± 0.165	-1.407 ± 0.201
HI_20160127045053	2.217 ± 0.003	2.718 ± 0.006	-24.953 ± 0.749	-27.726 ± 0.734	-20.31 ± 0.099	-22.771 ± 0.156	2.875 ± 0.275	-2.425 ± 0.178

3.1.4 Intercomparison

Based on the findings of RD-6, the measured range resolution of the PAZ data in Rosamond and Neustrelitz was usually similar or somewhat better than the provided values in the PAZ documentation, while the azimuth resolution was similar or slightly worse than the provided values. The measured localization errors were usually larger than the provided value, especially in range direction. We suspect that the same increase of the expected localization error from the nominal 2 m to the actual 2-4 m due to the conditions of the passed media and incidence angle reported in the TSX documentation applies also to PAZ, even though this has not been mentioned in the PAZ documentation. If assuming the same 2-4 m expected localization error also for PAZ, the measured localization errors would be in line with the expected values. In Rosamond the PSLR and ISLR in range and azimuth directions were few decibels higher than the theoretical values calculated for the Hamming window with an alpha coefficient of 0.6. In Neustrelitz the measured PSLR and ISLR in azimuth direction were close to the theoretical values, whereas in the range direction they were somewhat higher than the theoretical values.

Table 15 summarizes the results of the IRF analyses performed for the PAZ, TSX and CSK missions. The table shows the most typical value, either the average of all measured values, or the most common value after ignoring exceptional results. The localization error of PAZ SC and TSX SC data measured with SNAP are in x-axis (West-East) and y-axis (South-North) direction, and not in range and azimuth SAR geometry.

For the SC imaging mode, a complete comparison of the IRF quality values was possible only between PAZ and CSK. The spatial resolution of 16.6-19.2 m for the PAZ SC data is significantly higher than the 29 m of CSK WR data. However, this difference is anticipated due to different imaging configurations. For both products the measured spatial resolution is within or even better than the expected values of 16.8-18.2 for PAZ and 30 m for CSK. Concerning PSLR and ISLR, the PAZ SC data shows generally better performance than the CSK, possibly due to different windowing method applied during the SAR data processing. The localization accuracy of PAZ seems to be better than the localization accuracies of TSX and CSK. The errors of PAZ measured in SNAP were almost half compared to the errors measured for TSX. The variation in the magnitude and direction of the localization errors for the different CSK acquisitions was quite large, while for PAZ and TSX the localization error of the different acquisitions was almost the same, indicating a higher precision (with a bias almost constant) of PAZ and TSX compared to CSK.

The IRF analyses of the SM data show very similar spatial resolution for all three missions, with slightly higher range resolution for PAZ and TSX, and slightly higher azimuth resolution for CSK. The side lobes of the SM data are very similar for PAZ and TSX which both apply the same hamming windowing in the SAR data processing, apart from the PSLR in range which is 3 dB higher for PAZ compared to TSX. As in the SC mode, also in the SM mode the side lobes of CSK are systematically stronger compared to PAZ, probably due to different windowing methods. The localization accuracy of the PAZ and TSX SM products are very similar, while for CSK the variation of the localization error and the magnitude in azimuth direction are larger compared to PAZ and TSX. For the SL and HS imaging modes, the spatial resolution and localization errors of PAZ were very close to the ones of TSX. For these imaging modes, the PSLR and ISLR in range direction was 2-7 dB stronger for PAZ, while the side lobes in azimuth direction were very similar for PAZ and TSX.

Generally, for all imaging modes, The IRF results show similar quality of PAZ and TSX, with somewhat better quality of PAZ concerning localization accuracy, but somewhat better quality of TSX concerning the side lobes in range direction. The available CSK data have generally weaker performance concerning the PSLR, ISLR and localization accuracy compared to PAZ and TSX, but are still in line with the CSK product specifications (Table 8).

Table 15: Summary of the IRF analysis for the PAZ, TSX and CSK missions. The values are given as averages or typical values measured for the different sensors and imaging modes.

Im. mode	Mission	Rg. Res [m]	Az. Res [m]	Rg. PSLR [dB]	Az. PSLR [dB]	Rg. ISLR [dB]	Az. ISLR [dB]	Rg. Loc. Error [m]	Az. Loc. Error [m]
SC	PAZ	16.6	19.2	-23	-27	-18	-21	4.1 (10 in SNAP)	-3.3 (-2 in SNAP)
	TSX							19 (in SNAP)	-4 (in SNAP)
	CSK	29	29	-19	-21	-15	-13	-6.2...8.4	-1.746 ± 0.161
SM	PAZ	1.75	3.0	-26	-30	-24	-25	2.6	0.2
	TSX	1.76	2.96	-29	-30	-25	-25	2.7	0.2
	CSK	1.8	2.8	-23	-27	-19	-23	-0.9...2.9	-2.4...-1.4
SL	PAZ	1.17	1.6	-25	-30	-23	-25	2.7	0.3
	TSX	1.18	1.57	-28	-30	-25	-25	2.8	0.2
HS	PAZ	0.6	1.1	-24	-30	-22	-25	2.5	0.2
	TSX	0.62	1.08	-31	-30	-26	-26	2.8	0.2

3.2 Equivalent Number of Looks (ENL)

The ENL analysis is typically performed over natural distributed homogeneous targets. In this analysis the test areas used for the analysis were in the Amazonas Rainforest, Antarctica Glacier and Sahara Desert (Sudan and Egypt). Rainforests are considered homogeneous targets, especially for X-band sensitive to tree canopies. Glaciers are also homogeneous targets which enable the testing of ENL. Deserts are homogenous targets and have a relatively low backscatter due to smooth and dry soil. Hence, they are primarily used for assessing the contribution of noise in the SAR images (NESZ). However, due to the homogeneous texture of the desert images, they can also be utilized for assessing the ENL.

All SC data of PAZ, TSX and CSK were in MGD/DGM processing mode, and the other acquisition modes in SSC/SCS processing mode. The ENL value for SSC/SCS should be close to 1, while the value for MGD/DGM depends on the multilook factor applied. Table 16 presents the number of SSC/SCS and MGD/DGM datasets for each analysed environment.

Table 16: The number of analyzed SSC/SCS and MGD/DGM scenes over the homogeneous targets; rainforest, glacier and desert, for PAZ, TSX and CSK.

Target	PAZ		TSX		CSK	
	SSC	MGD (SC)	SSC	MGD (SC)	SCS	DGM (SC)
Rainforest	5	1	8	2	6	2
Glacier	2	2	5	3	4	4
Desert	4	0	7	0	3	0

The ENL analysis is mainly performed using the SQT software, by manually choosing a sub-window containing homogeneous texture from the SAR backscatter image and applying the calculation of the ENL to the chosen window. For the TSX SC data the ENL was calculated similarly, but using the SNAP software. Figure 6 presents an example of a chosen sub-window in a PAZ SL scene from the Sahara Desert.

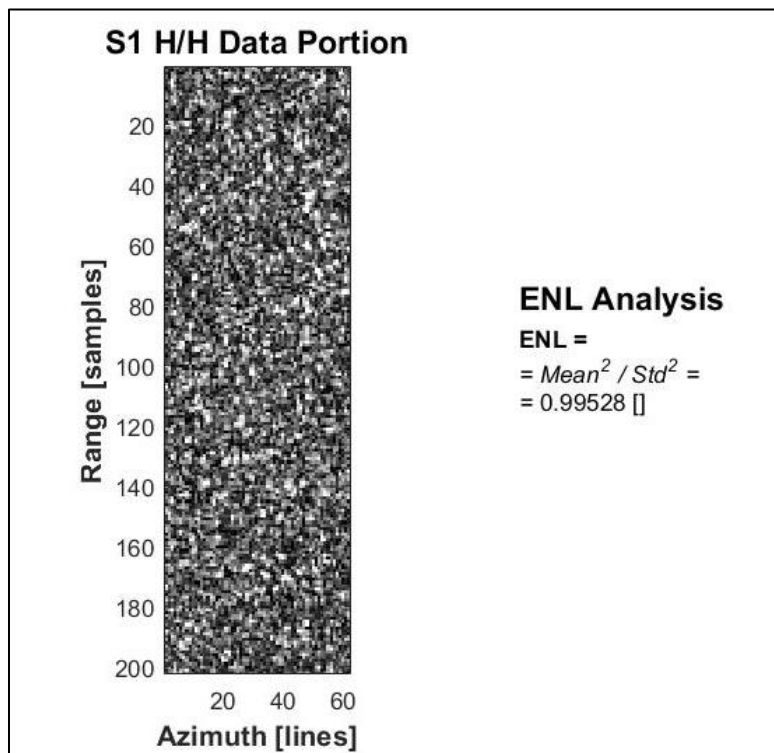


Figure 6. ENL analysis example for a PAZ SL scene, acquired at 13.9.2018.

3.2.1 PAZ

Table 17 shows the calculated and the ideal ENL (number of looks) for the PAZ scenes from the rainforests, glacier and the desert. The table shows the average and the standard deviation of the ENL values calculated from 5 sub-windows selected from each image.

Table 17: The measured and the ideal ENL for the PAZ data from the rainforest, glacier and desert areas. The average and the standard deviation of the measured ENL is calculated from 5 sub-windows for each image.

Test area	Date and time / (pol)	Im. mode	ENL	Number of looks (az*rg)
Rainforest	20180724T103235	SC	5.413 ± 0.179	5.25
	20180729T104201	SM	0.558 ± 0.013	1
	20180829T230505	SM	0.422 ± 0.015	1

	20190111T102407	SM	0.493 ± 0.075	1
	20180917T222156	HS	0.669 ± 0.09	1
	20180917T222316 / VV	SL	0.626 ± 0.026	1
	20180917T222316 / HH	SL	0.631 ± 0.022	1
Glacier	20190303T071204	SC	7.911 ± 0.232	8.74
	20190423T051400	SC	6.596 ± 0.088	6.52
	20180928T202612	SM	0.993 ± 0.008	1
	20180930T071214	SM	1.007 ± 0.006	1
Desert	20180924T034217 / HV	SL	0.976 ± 0.012	1
	20180924T034217 / HH	SL	0.944 ± 0.021	1
	20180913T034217	SL	0.96 ± 0.033	1
	20181122T161007	SM	0.958 ± 0.028	1
	20181111T161010	SM	0.952 ± 0.025	1

The derived ENL of the SC image from the rainforest was around 5.4, close to the ideal value of 5.25, which is the number of looks. The derived ENL for the SM, SL and HS rainforest scenes was between 0.6 and 0.7, meaning lower than the ideal value of ENL=1 for SSC. For the glaciers, the measured ENL of the SC MGD/DGM scenes is close to the number of looks, and the measured ENL of the SM scenes is very close to the ideal value of ENL=1. For the desert, all measured ENL values are close to one, as anticipated.

3.2.2 TSX

Table 18 shows the calculated and the ideal ENL (number of looks) for the TSX scenes from the rainforests, glacier and the desert. The table shows the average and the standard deviation of the ENL values calculated from 5 sub-windows selected from each image.

Table 18: The measured and the ideal ENL for the TSX data from the rainforest, glacier and desert areas. The average and the standard deviation of the measured ENL is calculated from 5 sub-windows for each image.

Test area	Date and time / (pol)	Pol	Im. mode	ENL	Number of looks (az*rg)
Rainforest	20170930T225010	HH	SC	2.888 ± 0.385	5.66
	20140804T102547	VV	SM	0.531 ± 0.009	1
		HH	SM	0.53 ± 0.011	1
	20140727T225642	VV	SM	0.509 ± 0.01	1
		HH	SM	0.51 ± 0.015	1
	20150318T101718	VV	SM	0.471 ± 0.011	1
	20140121T225707	HH	SM	0.457 ± 0.019	1
	20160329T105953	VV	SL	0.586 ± 0.053	1
		VV	SL	0.511 ± 0.038	1
	20100718T214726	HH	SL	0.509 ± 0.032	1
		VV	HS	0.347 ± 0.012	1
	20101130T090709	HH	HS	0.347 ± 0.012	1
		VV	HS	0.551 ± 0.03	1
	20090323T224949	HH	HS	0.563 ± 0.039	1
20171103T104230		HH	SC	3.401 ± 0.821	8.55
Glacier	20100512T152414	VV	SC	9.568 ± 0.514	9.57
	20150708T052253	HH	SC	6.852 ± 0.14	7.13
	20150708T113636	HH	SC	6.513 ± 0.344	7.14
	20071212T014106	VV	SM	0.993 ± 0.012	1
		VH	SM	0.995 ± 0.01	1
	20100310T222825	HH	SM	0.776 ± 0.032	1
		VV	SM	0.787 ± 0.013	1
	20200410T100716	VV	SM	0.993 ± 0.009	1
VH		SM	0.992 ± 0.008	1	

Desert	20100426T165313	VV	SM	0.991 ± 0.002	1
	20190718T025814	VV	SM	0.995 ± 0.003	1
	20071119T061733	HH	SL	0.592 ± 0.026	1
	20080820T164411	HH	SL	0.962 ± 0.014	1
	20100718T050705	VV	SL	0.978 ± 0.017	1
		HH	SL	0.978 ± 0.016	1
	20100513T050647	VV	SM	0.633 ± 0.161	1
		VH	SM	0.706 ± 0.142	1
	20100513T050655	VV	SM	0.979 ± 0.009	1
		VH	SM	0.999 ± 0.006	1
	20100907T164549	VV	SM	0.777 ± 0.005	1
		VH	SM	0.99 ± 0.008	1
	20101021T164549	VV	SM	0.852 ± 0.015	1
		VH	SM	0.997 ± 0.007	1

For the rainforests, the measured ENL of the TSX SC images were around 2.9 and 3.4, which are considerably lower than the ideal values (number of looks) of 5.7 and 8.6, respectively. The measured ENL was 0.46-0.53 in the SM data, 0.51-0.59 in SL and 0.34-0.56 in the HS data, meaning lower than the ideal value of one for SSC. For the glaciers, the measured ENL of the three SC MGD scenes is somewhat lower or close to the number of looks. The measured ENL of the SM scenes is typically higher than 0.99, thus very close to the ideal value of one, except for one SM scene from 20100310 showing relatively low ENL of 0.78. For the desert scenes, the measured ENL of the SM data varies between 0.63 and 1. For the SL images, the ENL was typically around 0.97, thus close to the ideal value of one, except for one scene with a measured ENL of 0.59.

3.2.3 CSK

Table 19 shows the calculated and the ideal ENL (number of looks) for the CSK scenes from the rainforests, glacier and the desert. The table shows the average and the standard deviation of the ENL values calculated from 5 sub-windows selected from each image.

Table 19: The measured and the ideal ENL for the CSK data from the rainforest, glacier and desert areas. The average and the standard deviation of the measured ENL is calculated from 5 sub-windows for each image.

Test area	Date and time	Im. mode	ENL	Number of looks (az*rg)
Rainforest	20170701104942	SC WR	2.975 ± 0.055	4.41
	20090217102245	SM	0.621 ± 0.053	1
	20090226225236	SM	0.56 ± 0.014	1
	20150120103357	SM	0.463 ± 0.014	1
	20191130220138	SM	0.469 ± 0.016	1
	20170324104356	SC WR	2.708 ± 0.083	4.36
	20180319220541	SM	0.522 ± 0.007	1
	20191126213637	SM	0.551 ± 0.04	1
Glacier	20130507102944	SC HR	14.28 ± 0.233	14.14
	20090611210407	SC HR	14.351 ± 0.168	14.14
	20090817005929	SC HR	14.26 ± 0.158	14.14
	20090817005929	SC HR	14.215 ± 0.231	14.14
	20111214183637	SM	0.986 ± 0.012	1
	20111222194259	SM	0.983 ± 0.006	1
	20130704063927	SM	0.991 ± 0.004	1
	20130727012923	SM	0.959 ± 0.038	1
Desert	20170401164520	SM	0.973 ± 0.021	1
	20170430164511	SM	0.965 ± 0.035	1
	20170409035633	SM	0,959 ± 0,025	1

For the rainforests, the measured ENL of the two SC WR images was 2.7-3.0, while the number of looks was around 4.4. The measured ENL of the SM HI images was between 0.46-0.62, meaning lower than the ideal value of one. For the glaciers, the measured ENL of all four SC HR DGM scenes is very close to the number of looks of 14.14, and the ENL of all SM HI images is close to the ideal value of ENL=1. For the desert scenes, the measured ENL of the SM data was always above 0.96, thus close to the ideal value of one for SSC data.

3.2.4 Intercomparison

For all three missions; PAZ, TSX and CSK, the measured ENL over rainforests was generally lower than the number of looks. For the SC MGD/DGM data though, the ENL of PAZ was somewhat closer to the ideal value compared to the TSX and CSK SC data. For the SSC/SCS data from rainforests, all missions showed ENL values considerably lower than the ideal value of 1. The measured lower ENL in rainforests for all missions indicates that although the rainforests can be considered spatially homogeneous for the X-band microwaves, they may not be homogeneous enough in the spatial scale required for proper ENL calculation. The glaciers provide a better solution for evaluating the ENL, as seen in the measured values for PAZ, TSX and CSK. In glaciers, the measured ENL of all missions and imaging modes showed values very close to the number of looks, apart from one exceptional scene for TSX. For the desert scenes, apart from few TSX scenes, the measured ENL was also close to the ideal value. The results from the Glacier and Desert sites indicate a correct radiometric processing of data for all the evaluated missions. The few exceptions among the TSX images might be related to images acquired from less homogeneous areas within the glaciers or the deserts.

3.3 Noise Equivalent Sigma Zero

One of the most essential quality indicators in SAR is the noise equivalent sigma zero (NESZ), showing the contribution of noise in the observed backscatter. Weaker NESZ is an indication of higher quality SAR data, because targets with relatively low backscatter can be identified with less noise disturbance. The NESZ is assessed using the SQT by manually extracting and plotting a range profile of the sigma nought (σ^0) backscatter from low backscatter areas. In an ideal case where there is no contribution of the target itself to the observed backscatter, the highest value of the range profile would be considered as the NESZ of the whole image, because it represents the worst-case scenario. However, in practice, the test areas are not ideal, and in most cases a small contribution of the target to the observed backscatter is expected. Hence, since there may be some residual backscatter even in the selected low backscatter areas, the minimum of the range profile is considered the NESZ value, assuming that the contribution of the target itself to the backscatter power is negligible. If the data contained two polarization bands, the band with the lower NESZ was considered. Figure 7 shows an example of a range profile extracted from one of the PAZ SM images over the Pacific Ocean.

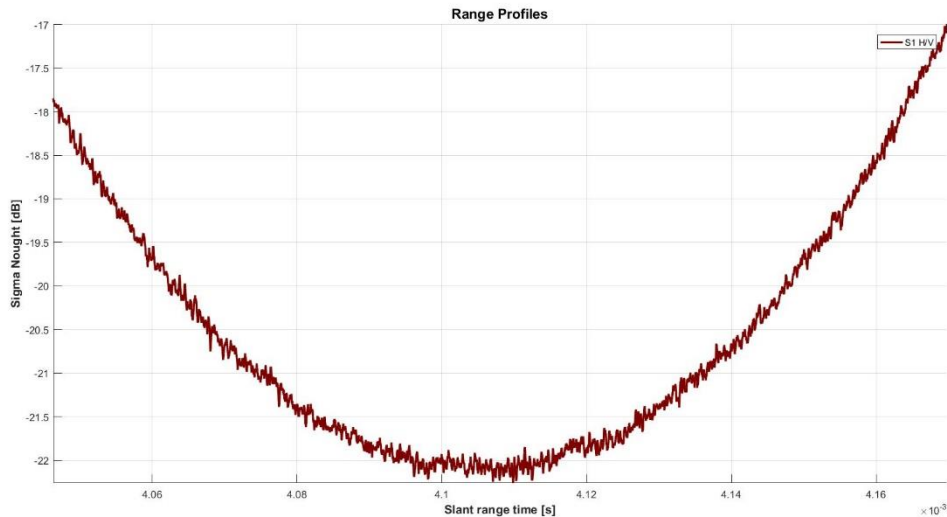


Figure 7: A range profile extracted from a PAZ SM scene over the Pacific Ocean acquired in 25.10.2018, for measuring the NESZ.

Table 20 shows the NESZ values for each product type provided in the PAZ documentation as an additional reference. The given NESZ values for PAZ are considered the worst case within the whole full performance incidence angle ranges. The measured NESZ of the PAZ test datasets should therefore be lower than the values in Table 20. The NESZ of all TSX test data used in this work given in the TSX documentation is -19 dB, and a NESZ range of -21...-22 dB is defined in the CSK documentation for all CSK data products.

Table 20: NESZ in decibels units (dB) of different products provided in the PAZ, TSX and CSK documentation.

Product type	Polarization	PAZ	TSX	CSK
ScanSAR MGD	Single	-18	-19	-21...-22
Stripmap SSC	Single	-16.8	-19	-21...-22
	Dual	-18.5	-19	-21...-22
Spotlight SSC	Single	-18.7	-19	-21...-22
	Dual	-16.5	-19	-21...-22
HR Spotlight SSC	Single	-16.2	-19	-21...-22
	Dual	-16.8	-19	-21...-22

3.3.1 PAZ

Table 21 shows the derived NESZ for the PAZ scenes acquired from water surfaces and from the desert. Over the water surfaces, the measured NESZ of the one single-pol SC and one dual-pol HS scene are -20 and -19.7 dB, respectively, and the NESZ of the SM scenes is -23.4 dB for the dual-pol and -22.2 dB for the single-pol scene. In the desert, the single-pol SM images have NESZ around -20.5 dB, and the SL scenes NESZ of -18.4 dB for the single-pol and -15.9 dB for the dual-pol scene.

Table 21: Measured NESZ for the PAZ data from water surfaces and desert.

Test area	Date and time (pol)	Im. mode	NESZ (dB)
Water surfaces	20181025T120434	SC	-20
	20181026T150743 (HV)	HS	-19.7

Desert	20181027T025940 (HV)	SM	-23.4
	20181025T033317	SM	-22.2
	20180924T034217 (HV)	SL	-15.9
	20180913T034217	SL	-18.4
	20181122T161007	SM	-21.5
	20181111T161010	SM	-19.7

3.3.2 TSX

Table 22 shows the derived NESZ for the TSX scenes acquired from water surfaces and from the desert. From the Doldrums, the measured NESZ of the one SC, one SL and one HS scene are -18, -3.6 and -20.7 dB, respectively. The SM scenes from the Doldrums show NESZ values between -22.2 and -6.9 dB. In the desert, the SM images have NESZ between -22.5 and -20.9 dB, and the SL scenes NESZ between -20.5 and -17.5 dB. We suspect that the few TSX scenes with very high NESZ are due to images from wavy water surfaces. Also, somewhat higher NESZ in some of the desert images might be due to higher surface roughness. If considering the data from both test areas, ignoring the scenes with supposedly wavy water or rough desert surfaces, the NESZ of the TSX data for the SC, SM, SL and HS modes can be estimated approximately -18, -22, -19 and -20.7 dB, respectively.

Table 22: Measured NESZ for the TSX data from water surfaces and desert.

Test area	Date and time (pol)	Im. mode	NESZ (dB)
Water surfaces	20200815T195315	SC	-18
	20160507T210632 (HH)	SM	-6.9
	20180815T074536	SM	-16.7
	20140923T203217	SL	-3.6
	20111211T193616	HS	-20.7
	20141017T085435	SM	-22.2
Desert	20071119T061733	SL	-17.5
	20080820T164411	SL	-18.3
	20100718T050705 (HH)	SL	-20.5
	20100513T050647 (VH)	SM	-22.1
	20100513T050655 (VV)	SM	-22.5
	20100907T164549 (VH)	SM	-20.9
	20101021T164549 (VH)	SM	-21

3.3.3 CSK

Table 23 presents the measured NESZ for the available CSK scenes. The two SC WR images show quite different NESZ, one with -26.1, while the other with -32.7 dB. The NESZ of the SM scenes for water surfaces and desert is between -18.7 and -23.6 dB, with approximately 2 dB lower NESZ in the desert compared to water surfaces.

Table 23: Measured NESZ for the CSK data from water surfaces and desert.

Test area	Date and time	Im. mode	NESZ (dB)
Water surfaces	20090602081626	SC	-26.1
	20160726062343	SC	-32.7

	20150427192048	SM	-21.8
	20150428202928	SM	-18.7
Desert	20170401164520	SM	-23.6
	20170430164511	SM	-23.1
	20170409035633	SM	-20

3.3.4 Intercomparison

As explained in RD-6, The NESZ of the PAZ scenes is generally at least 2 dB lower than the provided values in the PAZ documentation. Especially the SM images from the water surfaces show very low NESZ, more than 5 dB lower than the defined values in the documentation. As an exception, the SL dual-pol scene from the desert (acquired at 24.9.2018) shows NESZ somewhat higher than the defined -16.5 value, and the SL single-pol scene from the desert (acquired at 13.9.2018) shows slightly higher NESZ compared to the -18.7 dB provided in the PAZ documentation.

Table 24 show the average measured NESZ for each assessed acquisition mode and polarization combination of PAZ, TSX and CSK. Exceptionally high NESZ values of some TSX acquisitions are ignored, because they are most likely caused of wavy water surfaces significantly increasing in the target backscatter. For the SC, SM and SL single polarization imaging modes the NESZ of the PAZ data is 0.5-2 dB lower (better) than of the corresponding TSX data, whereas for the SL dual-pol, the NESZ of the TSX is more than 4 dB lower compared to PAZ. For the HS imaging mode, the NESZ of the TSX single-pol scene is 1 dB lower than of the PAZ dual-pol scene. Nevertheless, the TSX data shows generally good quality with respect to the reference NESZ provided in the TSX documentation. The NESZ of the CSK SM scenes is somewhat lower than the values measured for PAZ and TSX SM data, and the NESZ of the CSK SC scenes is significantly lower than in PAZ and TSX SC. This large difference can be related to different imaging configuration of CSK compared to PAZ and TSX. Regardless of the comparison with PAZ and TSX, CSK data is in line with the specifications provided in the CSK documentation.

It should be noted that for some imaging modes the variation of the measured NESZ between different scenes was quite high, indicating that some of the imaged areas were possibly not ideal low-backscatter surfaces for NESZ assessment, such as wavy water or rough desert sand/rock surfaces. Generally, we can conclude, that the quality in terms of NESZ is similar for PAZ and TSX, with somewhat better results for PAZ. CSK show better performance, especially for the SC mode, but this can be due to differences in imaging configurations.

Table 24: Comparison between the measured NESZ of PAZ, TSX and CSK for each imaging mode and polarization combination. The values represent averages of all relevant acquisitions, ignoring acquisitions with obviously exceptional NESZ. The values in parenthesis are the reference NESZ provided in the PAZ documentation, shown also in Table 20. The reference NESZ for all analysed TSX data is -19 dB, and for all CSK data between -21 and -22 dB.

Mission	SC	SM		SL		HS	
	Single	Single	Dual	Single	Dual	Single	Dual
PAZ	-20 (-18)	-21.1 (-16.8)	-23.4 (-18.5)	-18.4 (-18.7)	-15.9 (-16.5)		-19.7 (-16.8)
TSX	-18	-19.5	-21.6	-17.9	-20.5	-20.7	
CSK	-29.5	-21.4					

3.4 Antenna Elevation Pattern

The observed values need to be corrected for changes caused by the beam elevation angle in the range direction. A pre-defined antenna elevation pattern (AEP) is used by the data provider for compensating the contribution of the elevation angle to the measured gain. In this section we assess and compare the AEP correction applied on the PAZ, TSX and CSK data. The images were analysed by averaging the backscatter in azimuth direction and extracting range profiles of the averaged backscatter in slant range time units for SSC/SCS and in ground range distance for MGD/DGM products. The backscatter was then normalized by the inverse of the average measured backscatter. The analysis was performed on the Rainforest scenes, where the noise component can be considered negligible (very low) compared to the target backscatter level. Gamma nought (γ^0) backscatter was chosen because it is independent of the incidence angle with the ground surface. Ideally, the normalized γ^0 range profiles should be horizontal, with a value of zero dB along the x-axis.

3.4.1 PAZ

Figure 8 shows the normalized antenna pattern with respect to the slant range time or ground range distance, extracted from the analysed PAZ SAR images from the rainforests. The profiles show similar backscatter for the different elevation angles, with backscatter trend change of less than 0.5 dB from near to far range. Some spikes can be seen in the HS, SL and in two out of the three SM scenes, due to exceptional targets on the ground, such as rivers, forest cuts or roads. However, the general trend with respect to the elevation angle is nearly flat in all cases.

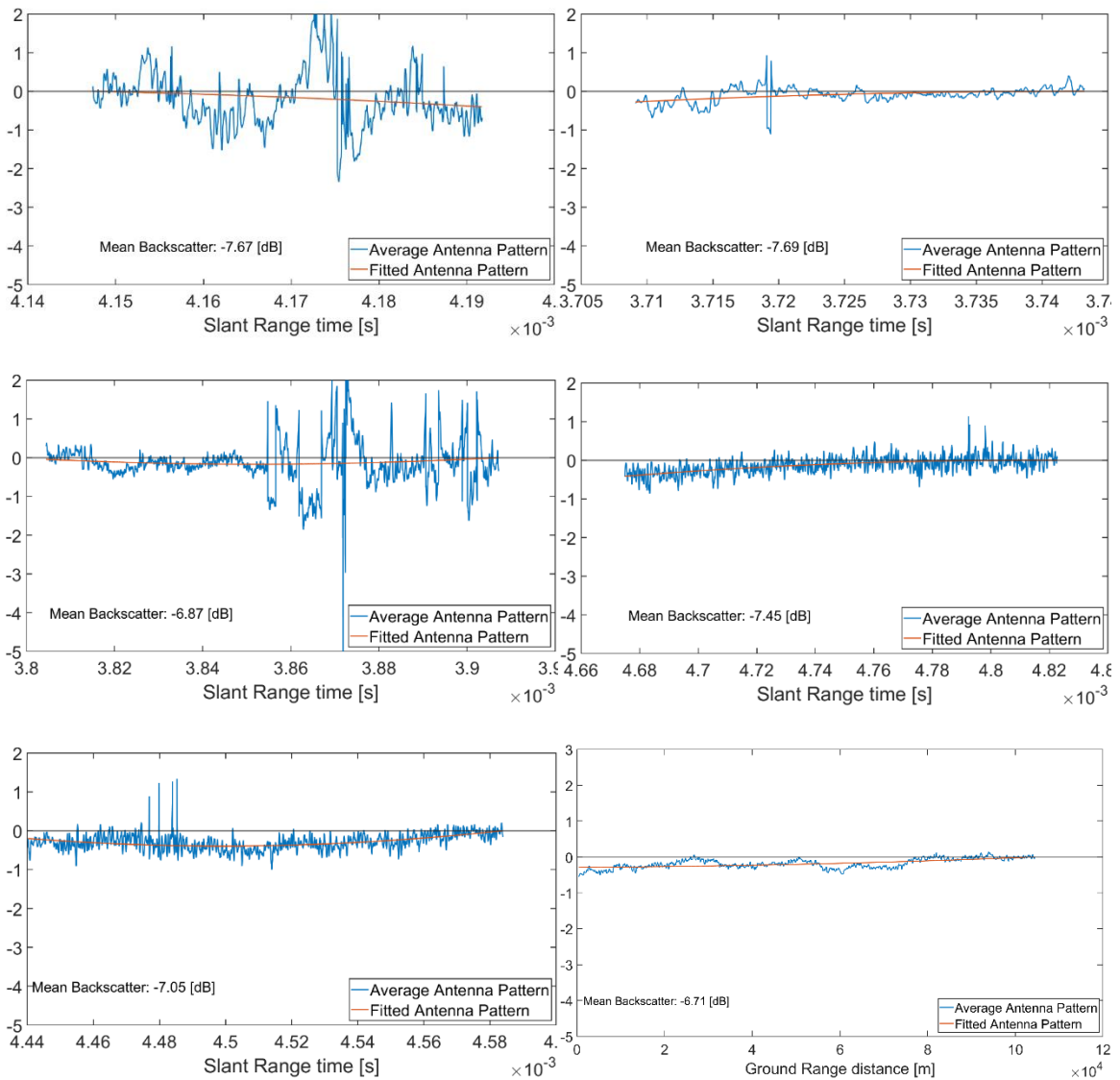


Figure 8: AEP of the PAZ scenes from the Amazonas Rainforest; HS scene acquired at 17.9.2018 (top-left), VV-polarization band of the SL scene acquired at 17.9.2018 (top-right), SM scene acquired at 29.7.2018 (middle-left), SM scene acquired at 29.8.2018 (middle-right), SM scene acquired at 11.1.2019 (bottom-left) and SC scene acquired at 24.7.2018 (bottom-right).

3.4.2 TSX

Figure 9 shows the normalized antenna pattern with respect to the slant range time or ground range distance, extracted from the analysed TSX SC and SM images from the rainforests. Apart from one SC scene, the profiles show nearly constant backscatter for the varying elevation angle, with nearly zero changes in the backscatter trend from near to far range. For one SC scene acquired at 3.11.2017, a linear trend with respect to range distance was observed, with a backscatter change of about 3 dB between near and far range.

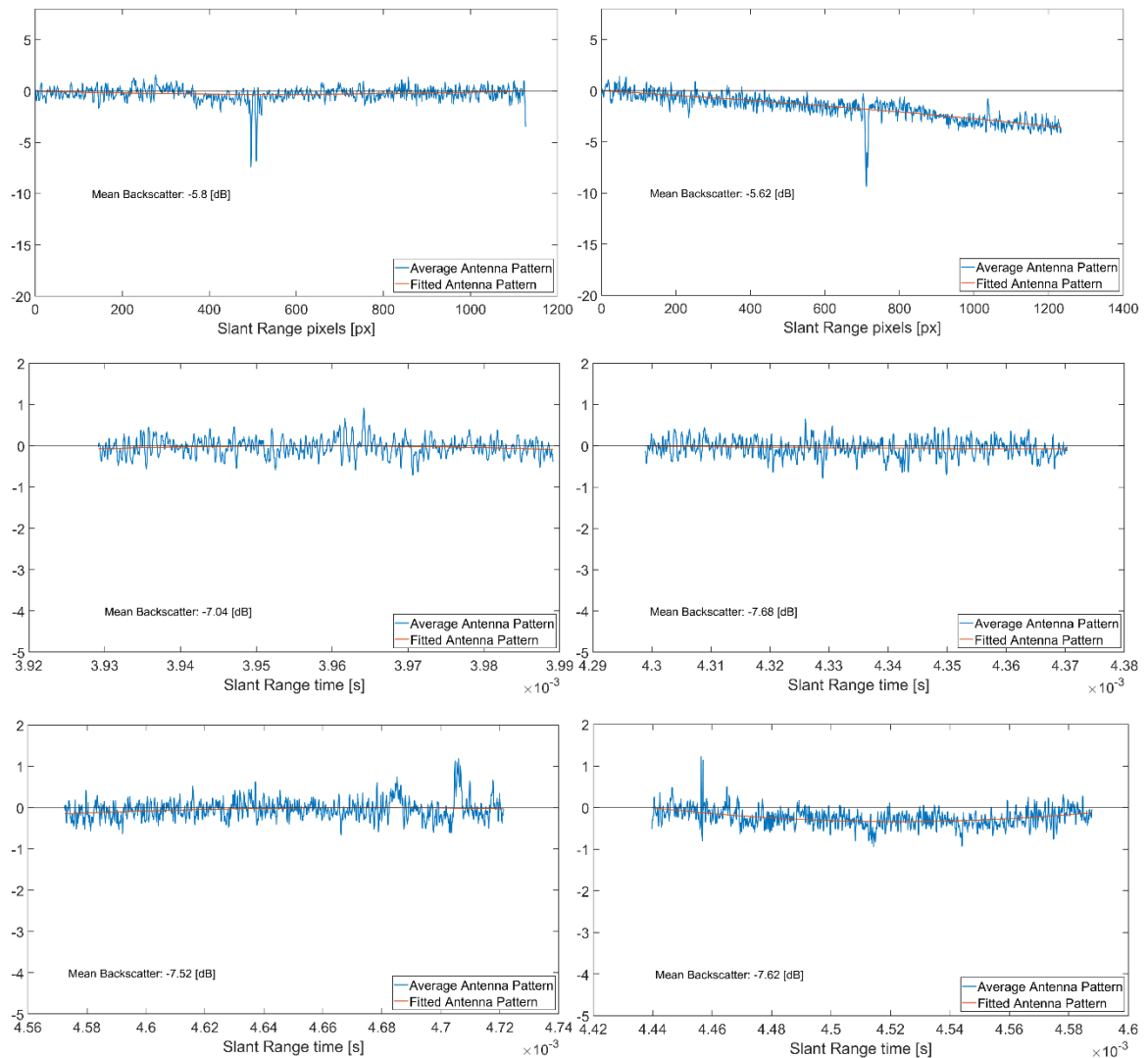


Figure 9: AEP of the TSX SC and SM scenes from the Amazonas Rainforest; SC scene acquired at 30.9.2017 (top-left), SC scene acquired at 3.11.2017 (top-right), SM VV-pol scene acquired at 4.8.2014 (middle-left), SM VV-pol scene acquired at 27.7.2014 (middle-right), SM scene acquired at 18.3.2015 (bottom-left) and SM scene acquired at 21.1.2014 (bottom-right).

Figure 10 shows the normalized antenna pattern with respect to the slant range time, extracted from the analysed TSX SL and HS images from the rainforests. Some spikes can be seen in the two SL and one HS scenes, due to exceptional targets on the ground, such as rivers, forest cuts or roads. Successful AEP correction can be seen for the HS image acquired at 30.11.2010, with a similar performance than in the SM scenes (Figure 9). The two SL scenes and the other HS scene acquired at 23.3.2009 show linear or almost linear backscatter trends with respect to varying elevation angle, with 1-2 dB change from near to far range.

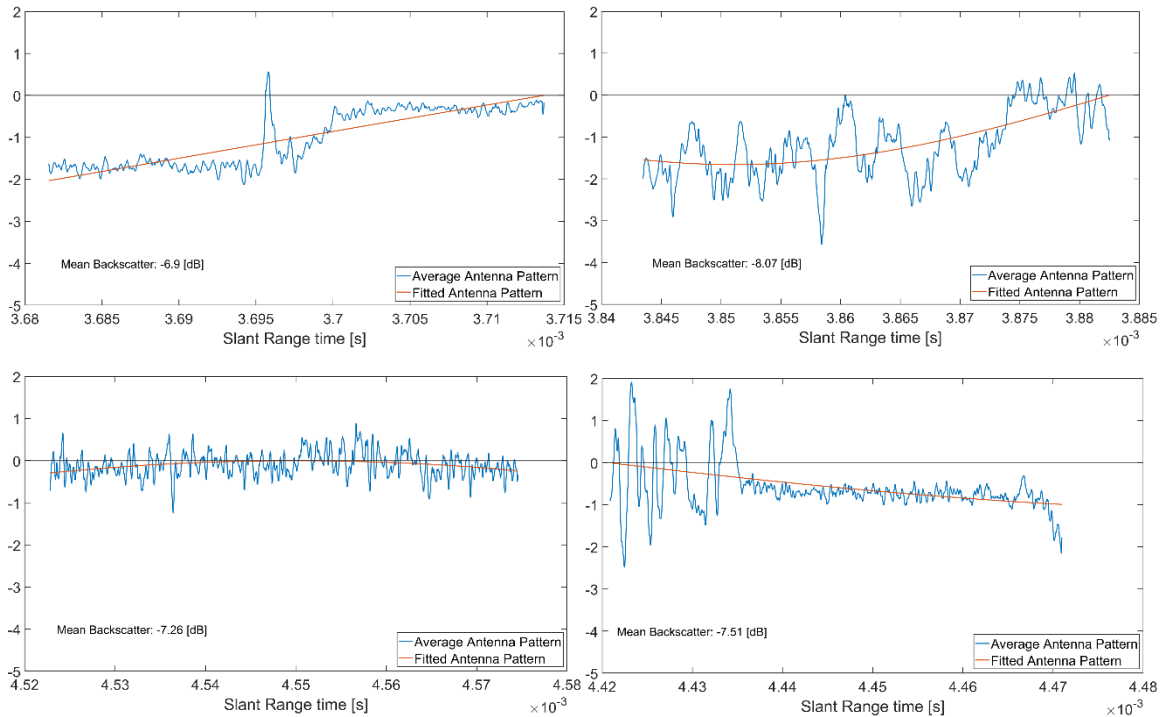


Figure 10: AEP of the TSX SL and HS scenes from the Amazonas Rainforest; SL scene acquired at 29.3.2016, VV-pol band of the SL acquired at 18.7.2010, VV-pol band of the HS scene acquired at 30.11.2010 and VV-pol band of the HS scene acquired at 23.3.2009.

3.4.3 CSK

Figure 11 shows the normalized antenna pattern with respect to the slant range time or ground range distance, extracted from the analysed CSK SAR images from the rainforests. In the SC scene acquired at 1.7.2017, the backscatter trend is generally horizontal for varying elevation angles, but with obvious increasing and decreasing behaviour within the range profile. Overall, for the whole scene, the AEP correction is therefore good, but variation within or between different bursts are seen. The second SC scene acquired at 24.3.2017 shows better calibration within or between different bursts, but in the far range a decrease of ~1 dB in the normalized backscatter trend is seen relative to the rest of the range profile.

For the SM imaging mode, three out of the six scenes show correct elevation patterns with generally horizontal profiles all along the range axis. The other three scenes have horizontal range profiles in the near to middle range, but the trend of the normalized backscatter decreases in the far range, with a total decrease of approximately 1 dB in the far range with respect to the near range.

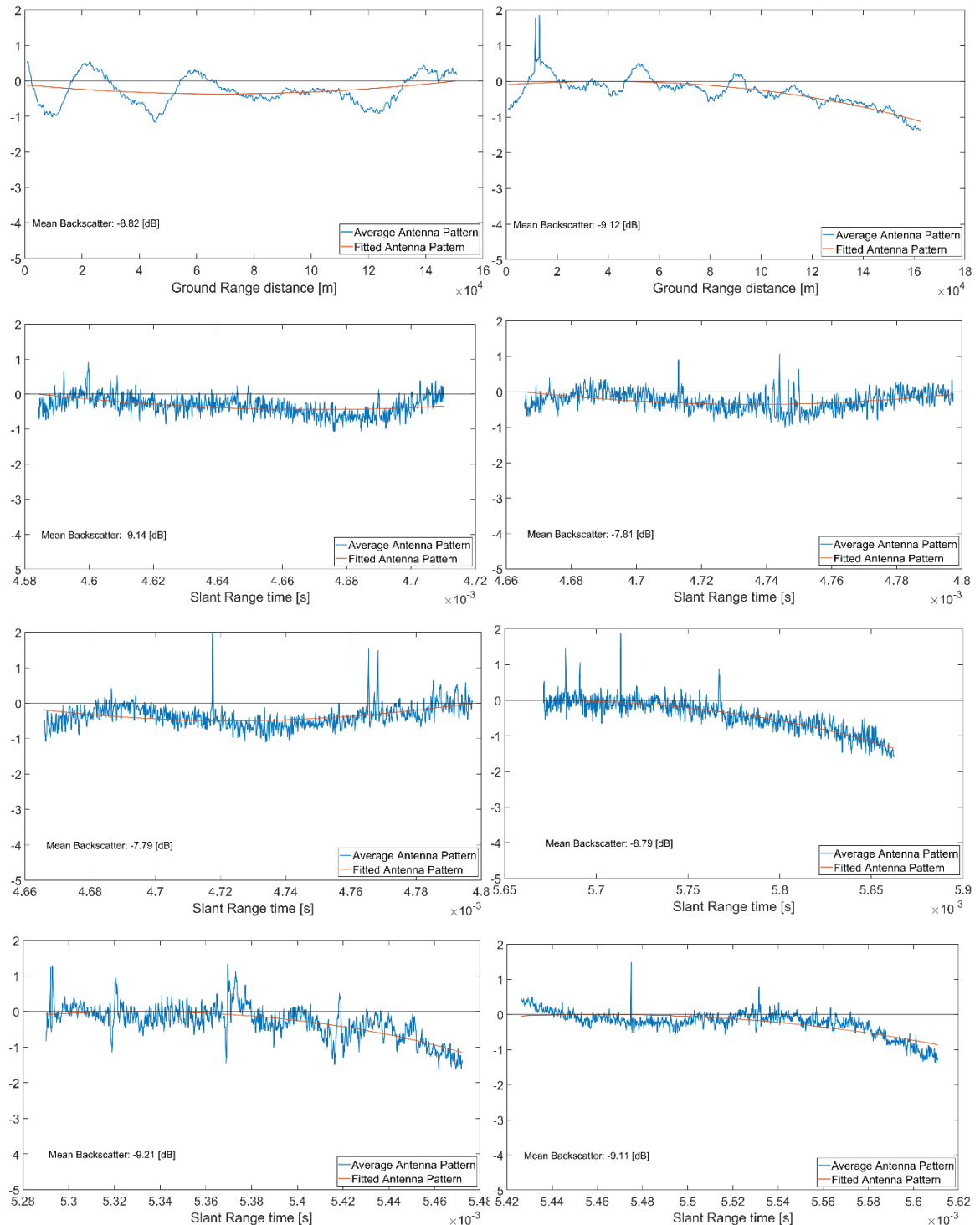


Figure 11: AEP of the CSK scenes from the Amazonas Rainforest. From left to right and top to bottom: SC scene acquired at 1.7.2017, SC scene acquired at 24.3.2017, SM scene acquired at 17.2.2009, SM scene acquired at 26.2.2009, SM scene acquired at 20.1.2015, SM scene acquired at 30.11.2019, SM scene acquired at 19.3.2018 and SM scene acquired at 26.11.2019.

3.4.4 Intercomparison

For the SC imaging mode, the number of analysed SC datasets was small; only one PAZ, two TSX and two CSK scenes. The one PAZ SC scene showed very good results in terms of the backscatter trend along the range direction but also in terms of radiometric similarity between the different bursts. From the two available TSX SC scenes, only one showed very good results, but the other one had a relatively large linear change of the backscatter with respect to the elevation angle. One of the CSK SC scenes had a general horizontal trend of the range profile, but the profile contained changes between the different bursts. The other CSK scene contained less variation between the bursts, but there was a decrease of the normalized backscatter towards the far range.

The number of analysed SM images was the largest for all three missions compared to the other imaging modes. Both PAZ and TSX showed good performance of AEP correction for all analysed SM data, whereas for CSK, half of the SM scenes showed good AEP correction, but half had a decrease of the normalized backscatter towards the far range. Therefore, based on the results obtained for the PAZ, TSX and CSK data in this work, we can conclude that the AEP correction has been applied overall more successfully for the PAZ data compared to TSX and CSK.

Concerning the very high resolution SL and HS data, the PAZ scenes had more successful AEP corrections compared to TSX. For PAZ, all data showed nearly horizontal backscatter trend all along the range axis, while in TSX, only one out of the four very high resolution images had the same performance. The other three TSX scenes had decreasing or increasing trends of 1-2 dB from near to far range.

4. CONCLUSIONS

An independent assessment and intercomparison of PAZ, TSX and CSK X-band SAR data quality was performed by FMI. The analysed PAZ and TSX data included SC, SM, SL and HS products, and the CSK data included SC and SM products. Data from the same, or at least similar locations were acquired, with imaging properties as similar as possible for the three data providers.

The relevant parameters describing the SAR data quality were retrieved mostly with the SQT software developed by Aresys, and in some cases with the SNAP software provided by ESA. The evaluated quality parameters were spatial resolution, peak side lobe ratio (PSLR), integrated side lobe ratio (ISLR), geolocation accuracy, equivalent number of looks (ENL), noise equivalent sigma zero (NESZ) and antenna elevation pattern (AEP). Especially the quality of PAZ and TSX was expected to be similar due to the same instrument platform. In a previous work reported in RD-6 we found that the measured quality of PAZ generally agrees with the stated values provided by Hisdesat in the PAZ documentation.

The results of the IRF analysis show similar quality of PAZ and TSX, although somewhat better localization accuracy for PAZ, and somewhat weaker (better) side lobes in range direction for TSX were measured. The available CSK data show generally weaker performance than PAZ and TSX concerning PSLR, ISLR and localization accuracy. The ENL analysis performed over the glaciers and the desert sites indicated correct radiometric processing of the PAZ, TSX and CSK data, but the ENL measured over the rainforests was lower than the ideal value for all three missions. Rainforests can be considered spatially homogeneous for the X-band microwaves, but it seems like they are not homogeneous enough in the spatial scale required for a proper ENL calculation. For most of the imaging modes the measured NESZ of PAZ was somewhat lower (better) than of TSX. CSK showed better performance, having lower NESZ values than PAZ and TSX, especially for the SC mode. The AEP correction applied for the PAZ data was usually more successful compared to TSX and CSK, apart from the SM data, where PAZ and TSX had very similar performance.

REFERENCES

- RD-1 SAR Level 1b Product Format Specification for PAZ SAR Processor. Available online: <https://www.hisdesat.es/en/documentos> (21.02.2022).
- RD-2 PAZ Image Product Guide, 2021. Available online: <https://www.hisdesat.es/en/documentos> (21.02.2022).
- RD-3 TerraSAR-X Product Guide, 2015. Available online: https://www.intelligence-airbusds.com/files/pmedia/public/r459_9_20171004_tsxx-airbusds-ma-0009_tsx-productguide_i2.01.pdf (21.02.2022)
- RD-4 TerraSAR-X Basic Product Specifications, 2013. Available online: <https://www.intelligence-airbusds.com/imagery/constellation/radar-constellation/technical-documents> (21.02.2022)
- RD-5 Italian Space Agency, COSMO-SkyMed, Mission and Products Description, 2016. Available online: [share.egeos-services.it/images/documents/COSMO-SkyMed Mission and Products Description.pdf](http://share.egeos-services.it/images/documents/COSMO-SkyMed%20Mission%20and%20Products%20Description.pdf) (21.02.2022)
- RD-6 PAZ Quality Assessment Summary, EDAP, 2022. Available online: <https://earth.esa.int/eogateway/documents/20142/37627/Technical+Note+on+Quality+Assessment+for+PAZ.pdf/0010668b-5f0b-416a-107f-2a2b7fe52a71> (22.02.2022)